Biophysical Journal
Article

Biophysical Society

Path sampling with memory reduction and replica exchange to reach long permeation timescales

Wouter Vervust,[1] Daniel T. Zhang,[2] Titus S. van Erp,[2] and An Ghysels[1,*]
[1]IBiTech – Biommeda Research Group, Faculty of Engineering and Architecture, Ghent University, Gent, Belgium and [2]Department of Chemistry, Norwegian University of Science and Technology, Trondheim, Norway

ABSTRACT Assessing kinetics in biological processes with molecular dynamics simulations remains a computational and conceptual challenge, given the large time and length scales involved. For kinetic transport of biochemical compounds or drug molecules, the permeability through the phospholipid membranes is a key kinetic property, but long timescales are hindering the accurate computation. Technological advances in high-performance computing therefore need to be accompanied by theoretical and methodological developments. In this contribution, the replica exchange transition interface sampling (RETIS) methodology is shown to give perspective toward observing longer permeation pathways. It is first reviewed how RETIS, a path-sampling methodology that gives in principle exact kinetics, can be used to compute membrane permeability. Next, recent and current developments in three RETIS aspects are discussed: several new Monte Carlo moves in the path-sampling algorithm, memory reduction by reducing pathlengths, and exploitation of parallel computing with CPU-imbalanced replicas. Finally, the memory reduction presenting a new replica exchange implementation, coined REPPTIS, is showcased with a permeant needing to pass a membrane with two permeation channels, either representing an entropic or energetic barrier. The REPPTIS results showed clearly that inclusion of some memory and enhancing ergodic sampling via replica exchange moves are both necessary to obtain correct permeability estimates. In an additional example, ibuprofen permeation through a dipalmitoylphosphatidylcholine membrane was modeled. REPPTIS succeeded in estimating the permeability of this amphiphilic drug molecule with metastable states along the permeation pathway. In conclusion, the presented methodological advances allow for deeper insight into membrane biophysics even if the pathways are slow, as RETIS and REPPTIS push the permeability calculations to longer timescales.

SIGNIFICANCE Permeability is a key kinetic property for membranes. Simulating permeation events at the molecular scale is very valuable for kinetic modeling, but permeation timescales are often prohibitively long to be simulated with present-day computational resources. Here, we show how the RETIS path-sampling method can give the exact kinetics of permeation, and how its efficiency is aided by recent developments. Moreover, we present a newly implemented REPPTIS method that approximates the kinetics by truncating memory. The REPPTIS method is promising for permeation simulations with high efficiency and accuracy that might not be easily achieved by any other method.

INTRODUCTION

Biological membranes are responsible for compartmentalization in cells and organelles. Their permeability is a key characteristic of the transport kinetics of chemicals and nutrients, peptide-membrane interactions, or drug delivery of nanocarriers (1–7). Molecular dynamics (MD) simulations are a computational tool that aid the understanding of the biophysical mechanisms playing at the molecular scale. Unfortunately, membrane permeability simulations are often computationally very demanding. The study of permeation events requires long timescales when the permeation is a slow and/or rare event, in addition to the need for fairly large simulation boxes usually comprised of thousands of particles. Permeability methods, such as the counting method (8–10) and the inhomogeneous solubility-diffusion model (11–13), are hence hindered by poor statistics. The latter approach can be combined with methods such as umbrella sampling (14) or adaptive biasing force (15,16) to obtain the free energy profile more efficiently. However, the possible presence of hysteresis and parallel reaction

Submitted October 7, 2022, and accepted for publication February 15, 2023.

*Correspondence: an.ghysels@ugent.be

Editor: Chris Chipot.
https://doi.org/10.1016/j.bpj.2023.02.021

channels can still sabotage an accurate description of the dynamics.

In recent work by some of the authors, an algorithm was proposed to evaluate the permeability with the path-sampling methodology, which realizes a speed-up of several orders of magnitude when the permeation event is rare (17). Path sampling, and in particular transition interface sampling (TIS) (18), achieves this speed-up by Monte Carlo (MC) sampling of path ensembles that are populated mostly with reactive paths or paths that make substantial progression along the reaction coordinate before returning to the reactant state. It was derived how the permeability can be obtained from the replica exchange transition interface sampling (RETIS) method (17). The method does not need a diffusive assumption, and the kinetics are thus exact.

Other notable methods that try to determine dynamic quantities, faster than MD, are milestoning (19) and forward flux sampling (FFS) (20). The latter is based on the same theoretical foundations as TIS, but instead of Metropolis MC sampling (21), it is based on splitting. In this class of methods, phase points of trajectories far up the barrier are used to launch multiple trajectories that deviate from the original due to the stochastic nature of the dynamics. Some of these trajectories reach further and deliver new phase points for launching the next set of trajectories and so on. Although the FFS method has the advantage over TIS and RETIS that it can be applied for nonequilibrium dynamics, the splitting technique has as a major disadvantage in that the final transition trajectories can be highly correlated and that possibly important rare initial conditions with a high reaction probability are missed (22). Milestoning, on the other hand, has the advantage that the statistics of long transition paths is obtained via the transition probabilities of much shorter paths connecting so-called milestones. The method bears resemblance to the simultaneously introduced TIS variation called partial path TIS (PPTIS) (23). Unlike the TIS, RETIS, and FFS methodologies, both PPTIS and milestoning are generally not exact as they rely on a memory loss assumption (Markovian approximation). Only in the hypothetical case that the milestones/interfaces are identical to isocommittor surfaces do these two methods become exact (24). In any other case, the inclusion of some memory can improve the accuracy of the method, which we discuss later.

Of the above methods, milestoning has been most commonly used to calculate permeability through membranes via slightly different theoretical approaches based on Markovian approximations (25–28). We recently derived how the permeability can be computed from a RETIS simulation that is not based on a disturbance out of equilibrium or Markovian assumptions (17), but, instead, it reproduces exact results identical to the counting method in a hypothetically long equilibrium MD run.

RETIS has been shown to provide the permeability for a range of toy systems (17). Moreover, RETIS was successfully used in a realistic simulation setup to compute the permeation rate of oxygen molecules through a 1-palmitoyl-2-oleoyl-*sn*-glycero-3-phosphocholine membrane (29). Nevertheless, for systems with slow permeation events, where the permeation trajectories sampled in the path ensembles occasionally are very long, the RETIS simulation can still be computationally demanding. To reach such long timescales, further methodological improvements are needed to improve sampling and efficiency.

This paper starts with a short review on how the permeability formula is derived from RETIS. Next, we give an outlook on how the simulations at these long timescales can be made more efficient. For permeation events with very long pathlengths, a lower computational cost may be obtained with a reduction of memory similar to milestoning and PPTIS. Specifically, we extend the PPTIS method with a replica exchange move between path ensembles to enhance nonlocal sampling. Other improvements for the sampling efficiency are reviewed as well, such as the use of special path-generating MC moves (17,30,31) and a new way to run replica exchange simulations with cost-unbalanced replicas with an infinite swap frequency (32).

The set of these methodological advances in three areas, i.e., memory reduction, new Monte Carlo moves, and parallel computing, will push permeability calculations to longer timescales. Specifically, the methodology that shortens memory is illustrated in the results using two example systems. In the first system, a permeant needs to pass through a maze-like membrane, choosing between a pathway with an entropic barrier and another pathway with an energetic barrier. The role of memory for PPTIS is challenged in this setup, as the memory loss might induce an overestimation or underestimation of the permeability compared with RETIS. In the second example, ibuprofen permeation through a bilayer is modeled. This drug molecule is amphiphilic, with a polar part (carboxylic group) and apolar part. The polar group creates metastable states in ibuprofen's permeation pathway, which can cause the trajectories to be trapped, making it an excellent application of memory reduction to keep the trajectory lengths short. The last section summarizes the conclusions.

METHODS

Permeability from RETIS

A RETIS simulation requires the definition of an order parameter λ and $n+1$ interfaces $\lambda_A = \lambda_0 < \ldots < \lambda_i < \lambda_n = \lambda_B$ to describe the progression of the reaction. For a permeability calculation, the order parameter is simply the coordinate of a specific "target" permeant, orthogonal to the membrane plane, so $\lambda = z_t$ in Fig. 1. In curved membranes, such as liposomes, λ could be chosen as the radial distance (33). In this subsection, a short overview of the permeability derivation is given to introduce the quantities that are needed to compute

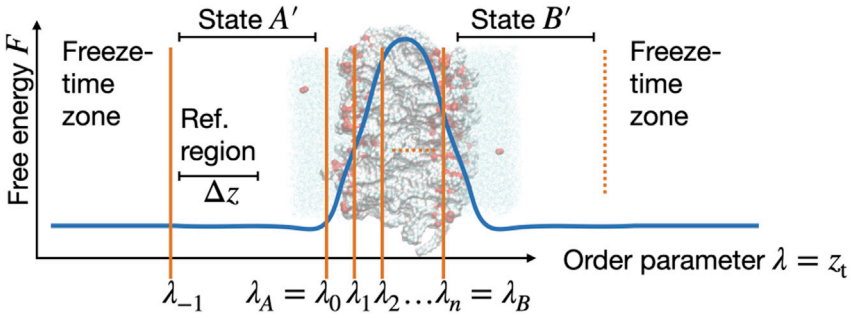

FIGURE 1 The membrane region between state A and state B forms a free energy barrier. Order parameter λ is the z_t coordinate of the target permeant normal to the membrane. RETIS interfaces $\lambda_A = \lambda_0, \ldots, \lambda_n = \lambda_B$ are indicated with orange lines. Additional interface λ_{-1} reduces region A to region A′ by freezing the time. Reference interval Δz is used to measure $\tau_{\mathrm{ref},[0^-{}']}$ in Eq. 8 or $(\rho_{\mathrm{ref}})_{A'}$ in Eq. 9. To see this figure in color, go online.

the permeability for the numerical applications in the next subsection.

A RETIS simulation consists of a series of path-sampling simulations (34), each employing a different path ensemble. There are $n + 1$ path ensembles called $[0^-]$, $[0^+]$, $[1^+]$, $[2^+]$, …, $[(n-1)^+]$. The $[0^-]$ ensemble explores the reactant well and consists of paths starting and ending at λ_0 with all other path frames being at the left side of this interface ($< \lambda_0$). All other path ensembles $[i^+]$ with $0 \leq i < n$ explore the barrier region and consist of paths starting at λ_0, ending at either λ_0 or λ_n, and crossing interface λ_i at least once. Since the path-sampling algorithm is based on MC moves obeying detailed balance, the set of trajectories that is being sampled in each path ensemble is statistically equivalent to a set of trajectories one would get by cutting out the relevant segments from an infinitely long MD trajectory.

Based on the results of the path ensembles, the rate can be computed as

$$k = f_A P_A(\lambda_B|\lambda_A) \tag{1}$$

where f_A is the conditional flux through $\lambda_A = \lambda_0$ and $P_A(\lambda_B|\lambda_A)$ is the overall crossing probability, the chance that λ_B will be crossed after a positive crossing with λ_A without recrossing λ_A. The rate in Eq. 1 can be related to a frequency of transitions between history-dependent states, called *overall states*, $\mathscr{A}$ and $\mathscr{B}$. These overall states differ from the stable states A and B, which are defined as the phase space regions being at the left of λ_A and at the right of λ_B, respectively. The overall state $\mathscr{A}$ also includes ("trajectory-") phase points that are in between λ_A and λ_B, which were more recent in A than in B. Likewise, overall state $\mathscr{B}$ includes points in between λ_A and λ_B, which originate from paths that were more recently in B than in A. Thus, the overall states $(\mathscr{A},\mathscr{B})$ are larger than the stable states (A,B). The rate constant k is then defined as the number of $\mathscr{A} \to \mathscr{B}$ transitions in a hypothetical infinitely long equilibrium MD run divided by the time spent in $\mathscr{A}$.

The flux f_A in Eq. 1 is the frequency of positive crossing with λ_A under the condition that the system is in overall $\mathscr{A}$. In rare events, however, the more complicated term to compute in Eq. 1 is the overall crossing probability $P_A(\lambda_B|\lambda_A)$ since it usually is an extremely small number. In TIS, RETIS, and also FFS, it is computed from the following product expression:

$$P_A(\lambda_B|\lambda_A) = P_A(\lambda_n|\lambda_0) = \prod_{i=0}^{n-1} P_A(\lambda_{i+1}|\lambda_i) \tag{2}$$

where $P_A(\lambda_{i+1}|\lambda_i)$ is the history-dependent conditional crossing probability, which is the chance that, given a first time crossing with λ_i since leaving state A, λ_{i+1} will be crossed before λ_A. The distribution of first crossing points with λ_i since leaving state A, is generally not identical to the equilibrium distribution at λ_i. This aspect includes memory in the expression of Eq. 2 and makes it exact. Milestoning and PPTIS can be viewed as approximate ways to determine the crossing probability by removing or reducing the memory dependence between subsequent interfaces, respectively.

Similarly to the rate k (unit 1/time), the permeability P is a kinetic property (unit length/time). The membrane permeability P is defined as the ratio $J/\Delta c$, where J is the net flux through the membrane when a concentration gradient Δc is maintained over the membrane in steady state. Firstly, in the counting method, this ratio is evaluated by counting the membrane crossings in both positive and negative directions and by evaluating the ratio $P = (J^+ + |J^-|)/(2c_{\mathrm{ref}})$ of the bidirectional flux $J^+ + |J^-|$ through the whole membrane and the reference concentration c_{ref} in a long equilibrium MD simulation. Secondly, in the inhomogeneous solubility-diffusion model, the permeability is estimated assuming diffusive transport, as described by the Smoluchowski equation, giving

$$\frac{1}{P} = e^{-\beta F_{\mathrm{ref}}} \int_{-h/2}^{h/2} \frac{1}{e^{-\beta F(z)} D(z)} \mathrm{d}z, \tag{3}$$

with $\beta = 1/(k_B T)$ the inverse temperature, k_B the Boltzmann constant, T the temperature, h the membrane thickness, and F_{ref} the reference free energy in the solvent phase in region A. The position-dependent free energy $F(z)$ and diffusion $D(z)$ profiles along the membrane normal to that figure in the Smoluchowski equation may be fitted from equilibrium MD with Bayesian analysis (35,36) or a maximum likelihood estimation (37).

Let us now return to the path-sampling methodology. The ratio $P = J^+/c_{\mathrm{ref}}$ is evaluated, where J^+ is the flux in the positive direction and c_{ref} is the reference concentration in state A at the left of the membrane (see Fig. 1). As shown in (17), the definition of J^+ has similarities to the RETIS rate k,

$$\begin{aligned} J^+ &= \frac{\#(A\to M\to B)_{\text{all perm.}}}{T\sigma} \\ k &= \frac{\#(A\to M\to B)_{\text{target}}}{T_{\mathscr{A}}} \end{aligned} \tag{4}$$

where M refers to the membrane region, T is the simulation time of a very long equilibrium simulation, $T_{\mathscr{A}}$ is the part of simulation time spent in overall state $\mathscr{A}$, and σ is the cross-section area of the membrane. By juggling Eqs. (4) and (1), it follows that

$$J^+ = f_A\, p_{\mathscr{A}}\, \frac{N_p}{\sigma}\, P_A(\lambda_B|\lambda_A) \tag{5}$$

with N_p the number of permeants in the simulation box and $p_{\mathscr{A}} = T_{\mathscr{A}}/T$. The quantity $p_{\mathscr{A}}$ in Eq. 5 is the probability that the permeants were last in state A rather than in state B. Its evaluation would necessitate full sampling of $\mathscr{B}$, which is, however, not sampled at all in the RETIS simulation! Fortunately, this factor conveniently drops out when evaluating the product $f_A p_{\mathscr{A}}$. This is a key point in the derivation of the practical permeability formula (see (17)). In a last step, the reference concentration c_{ref} enters in the ratio J^+/c_{ref}. It negates the N_p/σ factor in Eq. 5. When combined with the product $f_A p_{\mathscr{A}}$, the reference concentration contribution to the permeability formula becomes a matter of counting the time spent in a user-chosen reference interval Δz in state A. With the details given in (17), this gives an equation for the permeability that purely uses RETIS quantities,

$$P = \frac{\Delta z}{\tau_{\mathrm{ref},[0^-]}} P_A(\lambda_B|\lambda_A) \tag{6}$$

where $\tau_{\mathrm{ref},[0^-]}$ is the time spent in Δz, per path in the $[0^-]$ ensemble.

Yet, Eq. 6 is not straightforward to use with RETIS in practical simulations. The bulk phases at each side of the membrane are, in principle, unbounded such that the order parameter λ can have any value from minus infinite to infinite. The application of periodic boundary conditions will prevent this in practice, but could potentially introduce artificial transitions where a permeant ends up at the other side of the membrane without actually moving through it. Ghysels et al. (17) solved both issues by introducing an extra interface $\lambda_{-1} < \lambda_0$ that bounds region A to the left (Fig. 1). Time is frozen for particles that reach beyond λ_{-1}.

When using the λ_{-1} interface, the $[0^-]$ ensemble is replaced with the $[0^{-\prime}]$ path ensemble. Whereas $[0^-]$ only contains paths starting and ending at λ_0, the $[0^{-\prime}]$ ensemble will also contain paths that start or end at the other side of the A′ region, at λ_{-1}. Consequently, this changes the number of paths in $[0^{-\prime}]$ vs. $[0^-]$ that could be cut off a long equilibrium trajectory. This in turn affects the time spent *per path* in the Δz reference interval by a factor ξ, $\tau_{\mathrm{ref},[0^-]}\,\xi = \tau_{\mathrm{ref},[0^{-\prime}]}$ with

$$\xi = \frac{N_{\to R,[0^{-\prime}]}}{N_{[0^{-\prime}]}} \tag{7}$$

The factor ξ expresses this ratio in the number of paths between ensembles, i.e., only the paths arriving to the right at λ_0 are counted, versus all paths arriving at either λ_{-1} or λ_0 are counted. Using the factor ξ, this leads to the final permeability formula in presence of the λ_{-1} interface,

$$P = \frac{\xi \Delta z}{\tau_{\mathrm{ref},[0^{-\prime}]}} P_A(\lambda_B|\lambda_A) \tag{8}$$

Alternatively, one can write (17).

$$P = \frac{\xi P_A(\lambda_B|\lambda_A)}{(\rho_{\mathrm{ref}})_{A'}\,\tau_{[0^{-\prime}]}} \tag{9}$$

where $\tau_{[0^{-\prime}]}$ is the average pathlength of paths in ensemble $[0^{-\prime}]$ and $(\rho_{\mathrm{ref}})_{A'}$ is the conditional probability density of the reference region provided that the system is inside state A′. If both λ_0 and λ_{-1} are in the bulk where the free energy is flat, then $(\rho_{\mathrm{ref}})_{A'} = 1/(\lambda_0 - \lambda_{-1})$.

Improvements of sampling and computational efficiency

Reformulating the permeability expression in RETIS terminology has the obvious advantage that many recent developments in the RETIS method can now be used for permeation simulations. Recently, there have been some interesting advancements in the exact RETIS approach, but even further acceleration while maintaining a good accuracy is possible by reducing the memory dependency of the methodology via a PPTIS-like description of the crossing probabilities. In the next section, we present some simulation results on the combination of replica exchange and PPTIS, coined REPPTIS, in a highly simplified didactical model showing both the importance of replica exchange and memory. In this section, we cover the three aspects by which improvements toward longer timescales are achieved, i.e., development of new MC moves, novel parallelization schemes, and memory reduction.

MC moves

Like any MC method, the efficiency of the sampling highly depends on the types of moves that are being employed. Until recently, the main MC move in all path-sampling simulations has been the *shooting move* (38) in which a phase point of the previous trajectory is perturbed, usually by a randomization of the velocities alone, after which the equations of motion from this point are integrated forward and backward in time by means of MD until the boundaries of the stable

states, λ_A or λ_B, are hit. To ensure detailed balance, the final trajectory is accepted or rejected using a Metropolis-Hastings scheme (21,39).

The *shifting move*, which adds a few steps at the end and removes a few steps at the start of the path or vice versa, was the most frequently executed move in the original TPS method. The standard RETIS (40,41) rate calculation method emerged via TIS (18) from transition path sampling (TPS) (38,42). TIS and RETIS allowed for flexible pathlengths, which made the shifting move both useless and redundant. The *time reversal move*, which simply inverts the direction of time in the old path, used to be employed regularly in path-sampling simulations (TPS, TIS, and RETIS). While it is not so useful in present-day simulation settings where the randomization of velocities in the shooting move is mostly fully randomized, independent of the previous velocities, it is still useful for other types of path analysis such as the predictive capacity identification of reaction triggers (43). RETIS improved the former TPS further via the introduction of the $[0^-]$ path ensemble, and it added the *replica exchange* move between neighboring path ensembles to the palette (41). New advances in path sampling seek to add more alternative moves, replace the main shooting move entirely, or gain greater efficiency by novel parallelization schemes and by optimizing the relative frequency of the moves' execution.

New MC moves

In particular, in (17) we added two MC moves, the mirror move and the target swap move, specifically for permeation simulations. The *target swap move* improves the exploration path space whenever more than one permeant is present in the simulation box. As RETIS studies transition from the λ_A to the λ_B interface defined by the z coordinate of a single target particle, $\lambda = z_t$, the presence of other permeants in the system merely affects the environment of the target permeant. The target swap move, however, uses the statistics of the other permeants more effectively by a random reassignment of the target. This new target permeant might be located in a different area of the simulation box, and thus higher sampling decorrelation is likely achieved. The *mirror move* (17) increases the sampling in periodic systems by completely mirroring the particle's coordinates in the xy plane, effectively changing the reaction coordinate from $\lambda = z_t$ to $\lambda = -z_t$ with respect to the original coordinates. This implies that permeation pathways through the membrane in both directions are sampled, which also improves sampling efficiency. Despite the fact that the target swap move and the mirror move only operate in the $[0^{-'}]$ path ensemble, the faster exploration in the directions orthogonal to the reaction coordinate are felt by all the other path ensembles due to the replica exchange moves between path ensembles, as was clearly illustrated in a membrane model with two unequal permeation channels (17).

Another promising trend is to change the main MC move itself via so-called *subtrajectory moves* (30,31). The main idea behind these moves is that successive paths, created by the shooting move, are correlated, which leads to a statistical inefficiency, $\mathcal{N}$, of several tens or hundreds of paths (40). Not saving every path, but saving every N_s-th path, with $N_s < \mathcal{N}$, will typically not lead to any loss in statistical precision in the final result as a lower number of stored paths, which is used in the analysis, is compensated by a reduction in the correlation between the paths that are saved. While this may be a good strategy to save disk capacity and time required for writing to disk, the subtrajectory moves go a step further by significantly reducing the number of MD steps for paths that do not need to be saved. The subtrajectory move is best combined with the *high-acceptance* technique (30,31).

Parallellization

Further efficiency gains without invoking any approximation or Markovian assumption can be achieved via a smart parallelization scheme and by maximizing the replica exchange swapping frequency (32). Parallel computing will typically distribute the same number of processing units per ensemble to carry out the computational intensive standard moves. This makes the parallelization of the RETIS method a nontrivial task as each path can have a different length and the average pathlength differs for each path ensemble. Standard RETIS simulations apply the replica exchange swapping moves and standard MC moves alternately. The swapping move is cheap, but requires that the ensembles involved in the swap have completed their previous move. This means that, if the standard moves in each ensemble require different computing times, several processing units have to wait for the slow ones to finish, i.e., the replicas are cost-unbalanced. Roet et al. (32) solve this problem through a fundamentally new approach to the generic replica exchange method in which ensembles are not updated in cohort.

Roet et al. (32) also show that the number of replica exchange moves, in between two shooting or subtrajectory moves, can effectively be set to infinite without having to do an infinite number replica exchange moves explicitly. While the idea of infinite swapping has been suggested before (44–47), a reformulation of the implicit infinite swapping problem in terms of permanents allows for a much better scaling with the number of interfaces. The non-cohort infinite replica exchange approach applied to RETIS, coined ∞RETIS, opens the way for massively parallel path-sampling simulations for computing rate constants (40), activation energies (48), permeability constants (17), and mechanistic analysis for reaction triggers (43,49).

Reduction in memory

Still, when the individual trajectories themselves are too long to be simulated, the statistics of long trajectories should be obtained via shorter ones without actually sampling any trajectory going all the way from λ_A to λ_B. This is essentially the idea behind milestoning (19) and PPTIS (23). This strategy will generally cause the method to be no longer exact

unless the interfaces are isocommittor surfaces (24). However, the isocommittor surfaces are generally not known and extremely difficult and costly to determine via simulations. The lack of knowledge about the isocommittor can be compensated by adding a bit of memory to the interface crossing probabilities. We denote the PPTIS path ensembles as $[i^{\pm}]$ (23). Trajectories in path ensemble $[i^{\pm}]$ are restricted by the λ_{i-1} and λ_{i+1} interfaces. They can start and end at either side, but should at least cross the middle interface λ_i once. From these path ensembles, two-directional *local* crossing probabilities are obtained, $p_i^{\pm}$, $p_i{}^{=}$, $p_i^{\mp}$, and $p_i^{\ddagger}$. Here, the lower sign refers to the past conditional direction and the upper sign refers to the measure of the probability in the future, measured from a point in time where λ_i is crossed for the first time since its latest crossing with either λ_{i-1} or λ_{i+1}. For instance, both $p_i^{\pm}$ and $p_i^{\ddagger}$ refer to the probability that λ_{i+1} is crossed earlier than λ_{i-1} (future condition) after a first crossing with λ_i. But their past condition is different and equal to "given it came from λ_{i-1}" and "given it came from λ_{i+1}," respectively. The local crossing probabilities with the same past condition add up to one: $p_i^{\pm} + p^{=} = p_i^{\mp} + p_i^{\ddagger} = 1$. Once a sufficient number of paths in the $[i^{\pm}]$ ensemble is sampled, the local crossing probability is determined by simply counting the appropriate paths with specific future and past conditions, e.g., $p_i^{\pm}$ is given by the number of paths starting at λ_{i-1} *and* ending at λ_{i+1} divided by the number of paths starting at λ_{i-1}.

The PPTIS formalism is based on recursive relations where the local crossing probabilities are linked to *global* crossing probabilities:

$$P_j^+ \approx \frac{p_{j-1}^{\pm} P_{j-1}^+}{p_{j-1}^{\pm} + p_{j-1}^{=} P_{j-1}^-}, P_j^- \approx \frac{p_{j-1}^{\mp} P_{j-1}^-}{p_{j-1}^{\pm} + p_{j-1}^{=} P_{j-1}^-} \qquad (10)$$
$$P_1^+ = P_1^- = 1$$

where $P_j^+ = P_A(\lambda_j|\lambda_1)$ is the chance to cross λ_j before $\lambda_A = \lambda_0$ given that λ_1 is crossed at this moment while λ_A was crossed more recently than λ_1. Similarly, P_j^- is the chance that λ_A is crossed before λ_j given that λ_{j-1} is crossed at this moment while λ_j was crossed more recently than λ_{j-1}. From these recursive relations, the *overall* crossing probability from λ_A to λ_B can be computed from

$$P_A(\lambda_B|\lambda_A) = P_A(\lambda_n|\lambda_0) = P_A(\lambda_1|\lambda_0) P_A(\lambda_n|\lambda_1) = p_0^{\pm} P_n^+ \qquad (11)$$

Here, the $p_0^{\pm}$ probability is slightly different from the $p_i^{\pm}$ definitions with $i > 0$ in the sense that it is just the probability to reach λ_1 before λ_0 after a positive crossing with λ_0, i.e., $p_0^{\pm}$ has no additional past condition.

The larger the distance between interfaces, the more memory is included in the calculation, the more accurate is Eq. (10). The calculation of memory loss functions is a way to estimate the required distance between interfaces (23). On the other hand, the interfaces should be placed relatively close to each other to obtain the best efficiency. This can lead to conflicting strategies for parameter optimization. A potential solution could be to use path history beyond the boundaries of the $[i^{\pm}]$ ensemble. This kind of information could in principle become available if PPTIS is also combined with replica exchange moves.

The potential of performing replica exchange between path ensembles was first suggested for PPTIS (48). Yet, this idea has so far never been put in practice. The replica exchange move $[i^{\pm}] \leftrightarrow [(i+1)^{\pm}]$ in PPTIS is more costly than the swapping move $[i^{+}] \leftrightarrow [(i+1)^{+}]$ in RETIS. In RETIS, full trajectories are swapped without the need to do additional MD steps. In PPTIS, it is first checked whether the $[i^{\pm}]$ path ends at λ_{i+1} and whether the $[(i+1)^{\pm}]$ path starts at λ_i. If not, the move is directly rejected. However, if so, the $[i^{\pm}]$ and $[(i+1)^{\pm}]$ paths are extended forward and backward in time, respectively. Subsequently, the extended paths are trimmed in accordance to the new path ensemble boundaries to which the paths are being transferred to.

This article presents the first applications of the replica exchange and PPTIS combination, which we coin REPPTIS. The algorithms are implemented in the PyRETIS code, which is readily available to be used in combination with other MD simulation packages such as GROMACS, OpenMM, or CP2K (50,51). The first application is a model system, showing both the importance of the replica exchange moves and the effect of memory. In the second application of ibuprofen permeation, we show how RETIS is challenged by metastable states, which can make the paths prohibitively long, whereas REPPTIS can be used to simulate full membrane transits. The results of these two examples are presented in the next section.

RESULTS

Permeation through a maze potential

A two-dimensional toy system is developed to demonstrate the role of memory in permeability calculations. A Langevin particle is permeating along the z direction from the water phase through the membrane (Fig. 2). The propagation of the permeation is measured by the z coordinate of the particle, so the order parameter is $\lambda = z$. The coordinate y describes the orthogonal degrees of freedom, which could be a general coordinate such as the orientation of the molecule or the local composition of heterogeneous membranes. Here, a membrane is chosen with different permeation pathways; for instance, corresponding to different regions of a heterogeneous membrane. The membrane is represented by a maze potential with two permeation channels (upper channel for $y > 0.5$, lower channel for $y < 0.5$). Passage through the lower channel is entropically unfavorable, as the lower channel is only accessible via an aperture at about $z = 0.44$. Passage through the upper channel requires the Langevin particle to

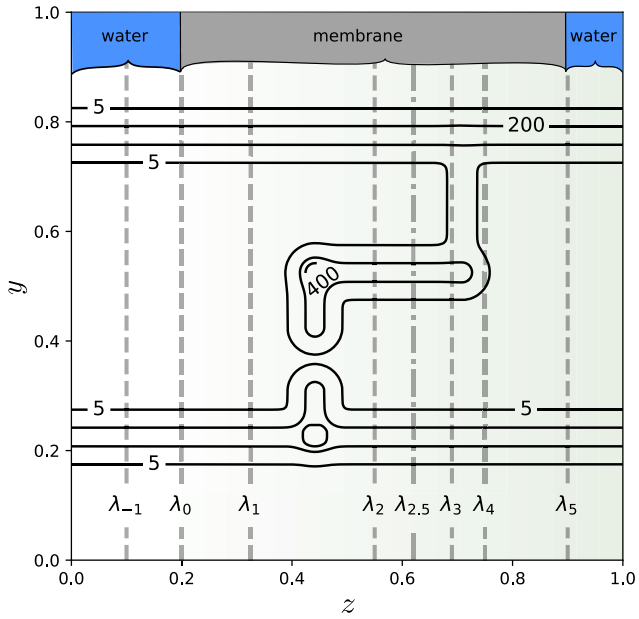

FIGURE 2 The potential energy $V(z, y)$ for the two-dimensional maze system. The isolines display the specific values for the potential. In addition, a green gradient is added in the horizontal direction from $z = 0.2$ to $z = 1.0$ to visualize the small, positive, and linear tilt with a slope of 0.5 that exists within that range in the potential. Interfaces $\lambda_{-1}, \ldots, \lambda_5$ are indicated with vertical dashed lines. Reduced units are used. To see this figure in color, go online.

overcome an energy barrier at $z = 0.71$. The maze can be thought of as a pinball machine, where the ball can either go through the "flippers" of the lower channel, or go over the "bump" in the upper channel. When the initial path is located in the upper channel passing over the bump, the orthogonal degree of freedom (y) will need to be sampled sufficiently with path sampling to detect the alternative pathway through the flippers, and vice versa. Moreover, for every z value, there is a broad y region in the upper and/or lower channel where the ball can easily move locally somewhat left or right. This local picture could give the impression that the ball has no entropic nor energetic challenges to overcome at all. However, all *complete* permeation pathways will need to overcome the entropic or energetic barrier, so including all memory in the pathways gives a distinctly different picture than the local picture. This makes our test case a good illustration of the role of memory. If one focuses on pieces of trajectories that only move somewhat to the left or right, i.e., if memory is too short, one will miss the dynamics included in the complete pathways.

We do different types of simulations.

- RETIS simulation, which retains all memory and thus gives exact kinetics. This is the benchmark.
- PPTIS simulation, where memory is reduced. In the $[i^+]$ ensemble, paths that cross λ_i are cut short when they pass a neighboring interface at λ_{i-1} or λ_{i+1}.
- REPPTIS simulation, where memory is reduced and where replica exchange moves between the $[i^+]$ ensembles are allowed. This potentially incorporates additional memory (see previous section).

Six interfaces were chosen along the z axis ($\lambda_A = \lambda_0, \ldots, \lambda_5 = \lambda_B$) in the membrane region between $\lambda_A = 0.2$ and $\lambda_B = 0.9$. The $[0^+], \ldots, [4^+]$ path ensembles were sampled for a total of 100,000 MC moves with the PyRETIS code (50,51) using shooting moves, the wire fencing (31) variant of the subtrajectory moves with 6 subpaths, and replica exchange moves. The $[i^+]$ ensembles were sampled for (RE) PPTIS without wire fencing moves. In addition, the λ_{-1} interface was used at $z = 0.1$ to bound the region at the left of the membrane. The properties ξ and $\tau_{\mathrm{ref},[0^-]}$ with the reference interval set to [0.1,0.2] were computed from the $[0^-]$ path ensemble. Two PPTIS simulations were run, where the first was initialized with a reactive path through the lower entropic barrier, and the second with a reactive path through the upper energetic barrier. These PPTIS simulations are referred to as PPTIS 1 and PPTIS 2, respectively.

To challenge the memory reduction, we also run REPPTIS with an extra interface at $z = 0.62$ between λ_2 and λ_3, which we refer to as $\lambda_{2.5}$ in this text for convenience. For RETIS, extra interfaces typically increase the accuracy as more paths are sampled, and matching the probabilities can be done with higher accuracy. For (RE)PPTIS, however, the extra interface implies a more drastic cut in memory as some of the $[i^+]$ ensembles will span a smaller spatial area. The simulation without and with the extra $\lambda_{2.5}$ interface are referred to as REPPTIS 1 and REPPTIS 2, respectively.

A tilt potential with slope 0.5 was superimposed on the maze potential (green gradient in Fig. 2) for $z \geq 0.2$, mimicking a membrane barrier. Details about setup, simulations, and code to generate more general maze potentials are given in the supporting material. Reduced units are used, and reported errors are standard errors based on block averaging.

The maze: Effect of memory and replica exchange move

The average pathlength in the highest RETIS ensemble $[4^+]$ is 47.5, while the $[4^+]$ (RE)PPTIS ensembles have an average pathlength of about 3.8. The goal of reducing the length of the MD trajectories by memory reduction is thus clearly achieved. With Eq. 8, the permeability from RETIS is equal to 2.54×10^{-5} ($\pm 8\%$). To compare the effect of memory on this permeability value, this discussion will focus on the crossing probability $P_A(\lambda_B|\lambda_A)$, which is the only factor in Eq. 8 that may be affected by the memory reduction. The overall crossing probability is given in Table 1. We first discuss the simulations without the extra $\lambda_{2.5}$ interface. The PPTIS 1 and PPTIS 2 simulations

TABLE 1 Overall crossing probability through the membrane from $\lambda_A = 0.2$ to $\lambda_B = 0.9$, without and with extra interface $\lambda_{2.5}$

	Overall	Forward			Backward		
Simulation	$P_A(\lambda_B\|\lambda_A)$ $[10^{-4}]$	p_2^+	$p_{2.5}^+$	p_3^+	p_2^-	$p_{2.5}^-$	p_3^-
RETIS	2.65 ($\pm 5\%$)						
PPTIS 1 initial lower	6.44 ($\pm 17\%$)	0.41		0.54	0.45		0.63
PPTIS 2 initial upper	0.93 ($\pm 34\%$)	0.18		0.24	0.70		0.96
REPPTIS 1	2.14 ($\pm 12\%$)	0.19		0.47	0.56		0.66
REPPTIS 2 with $\lambda_{2.5}$	2.94 ($\pm 9\%$)	0.59	0.28	0.43	0.39	0.79	0.75

For PPTIS, the initial path was either in the upper (PPTIS 1) or lower (PPTIS 2) channel. The local crossing probabilities p^+ and p^- are given for some of the $[i^+]$ ensembles.

significantly overestimate and underestimate the crossing probability, respectively, by more than a factor of 2. The added replica exchange moves in REPPTIS 1 improve the crossing probability considerably. Fig. 3 plots the intermediate crossing probabilities $P_A(\lambda_i|\lambda_A)$ to reach λ_i, showing that the first deviations between the simulations start at λ_3, when the Langevin particle has entered the maze.

Let us look at the origin of these deviations by tracing some randomly selected exemplary paths in the different ensembles in Fig. 4. In the reference simulation, RETIS, the reactive paths in $[4^+]$ cross both the entropic and energetic barrier, where the particle prefers the "flippers" channel (lower) rather than the "bump" channel (upper).

In PPTIS 1, the initial path is located in the lower channel and it remains there indefinitely in the $[3^+]$ ensemble. The MC shooting moves in $[3^+]$ cannot result in a switch to the other channel, so the path is stuck. The absence of such nonlocal moves that allow channel switching breaks the ergodicity of the sampling. The effect of this sampling deficit is modest as can be concluded from the p_3^+ and p_3^-

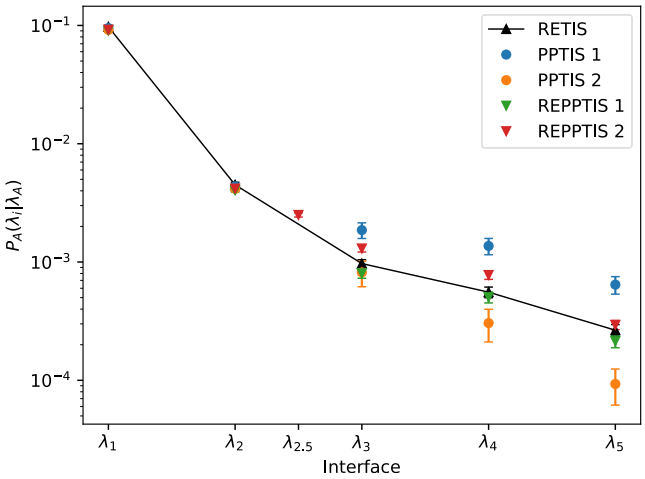

FIGURE 3 Crossing probabilities $P_A(\lambda_i|\lambda_A)$ for RETIS (*black*), PPTIS (*circles*), and REPPTIS (*triangles*) simulations. The RETIS simulation provides the benchmark values, which are connected by a line. REPPTIS 2 includes the extra $\lambda_{2.5}$ interface. Values to the right are the global crossing probabilities $P_A(\lambda_5|\lambda_A) = P_A(\lambda_B|\lambda_A)$. The error bars are standard errors based on block averaging. To see this figure in color, go online.

values in Table 1 since crossings with λ_3 are more likely in the lower channel where the potential energy is low. Also in the $[2^+]$ ensemble, the paths remain for most of the simulation in the lower channel, but here the ergodicity problem is more severe since most first time crossings with λ_2 coming from λ_1 should be in the upper channel. As it is more difficult to reach λ_3 from λ_2 in the undersampled upper channel, p_2^+ is overestimated. For PPTIS 2, the initial path is in the upper channel and the absence of nonlocal MC moves again breaks the ergodicity of the sampling, where the paths in $[3^+]$ are now stuck in the upper channel. In REPPTIS 1, we have added the replica exchange moves and, impressively, this move reintroduces ergodicity. When the y axis is sampled in the $[0^-]$ ensemble, this effect can be transported to the other ensembles with the swap move. Adding the exchange move will thus effectively allow for switching between channels.

The crossing probabilities of PPTIS are affected by the particle being stuck in $[3^+]$ (or somewhat stuck in $[2^+]$) in a particular channel. It is much easier to reach λ_3 in the lower channel instead of the upper channel, where λ_3 is high uphill on the wall's slope. The true mechanism has a mixture of both pathways (see RETIS). This gives an overestimation of the $\lambda_1 \to \lambda_2 \to \lambda_3$ and $\lambda_2 \to \lambda_3 \to \lambda_4$ crossing probability by PPTIS 1 and an underestimation by PPTIS 2. Numerically, this is also reflected in the local crossing probabilities. A selection is shown in Table 1; other local crossing probabilities were not statistically different between the simulations, as expected. PPTIS 1 is mainly located in the easier flipper channel, and p_2^+ is overestimated by PPTIS 1 compared with REPPTIS 1 (0.41 vs. 0.19), which increases the overall crossing probability in PPTIS 1. Likewise, PPTIS 2 is mainly located in the more difficult bump channel, and p_3^+ is strongly underestimated by PPTIS 2 compared with REPPTIS 1 (0.24 vs. 0.47). In combination with the higher backwards p_2^- and p_3^- values, this results in a lower overall crossing probability. In a very long PPTIS simulation, the $[2^+]$ ensemble could eventually be correctly sampled, but the $[3^+]$ ensembles will remain stuck with paths resembling the initial path.

Finally, we discuss REPPTIS 2 with the extra interface at $\lambda_{2.5}$, which further reduces memory. Fig. 3 shows that the probability to reach λ_3 is overestimated, which can be expected because of tunneling between $[2^+]$ and $[2.5^+]$. In $[2^+]$, the particle can move freely in the upper channel, as it is not hindered by the energetic barrier located to the right of $\lambda_{2.5}$. In $[2.5^+]$, the particle can move freely in the lower channel, as it is not hindered by the entropic barrier located to the left of λ_2. This can also be seen in Fig. 4, where the LMR and RML example paths of $[2^+]$ and $[2.5^+]$ are predominantly located in the upper and lower channel, respectively. Connecting these two ensembles to derive a $\lambda_1 \to \lambda_2 \to \lambda_3$ crossing probability, the particle seems to switch from the upper channel in $[2^+]$ to the lower channel

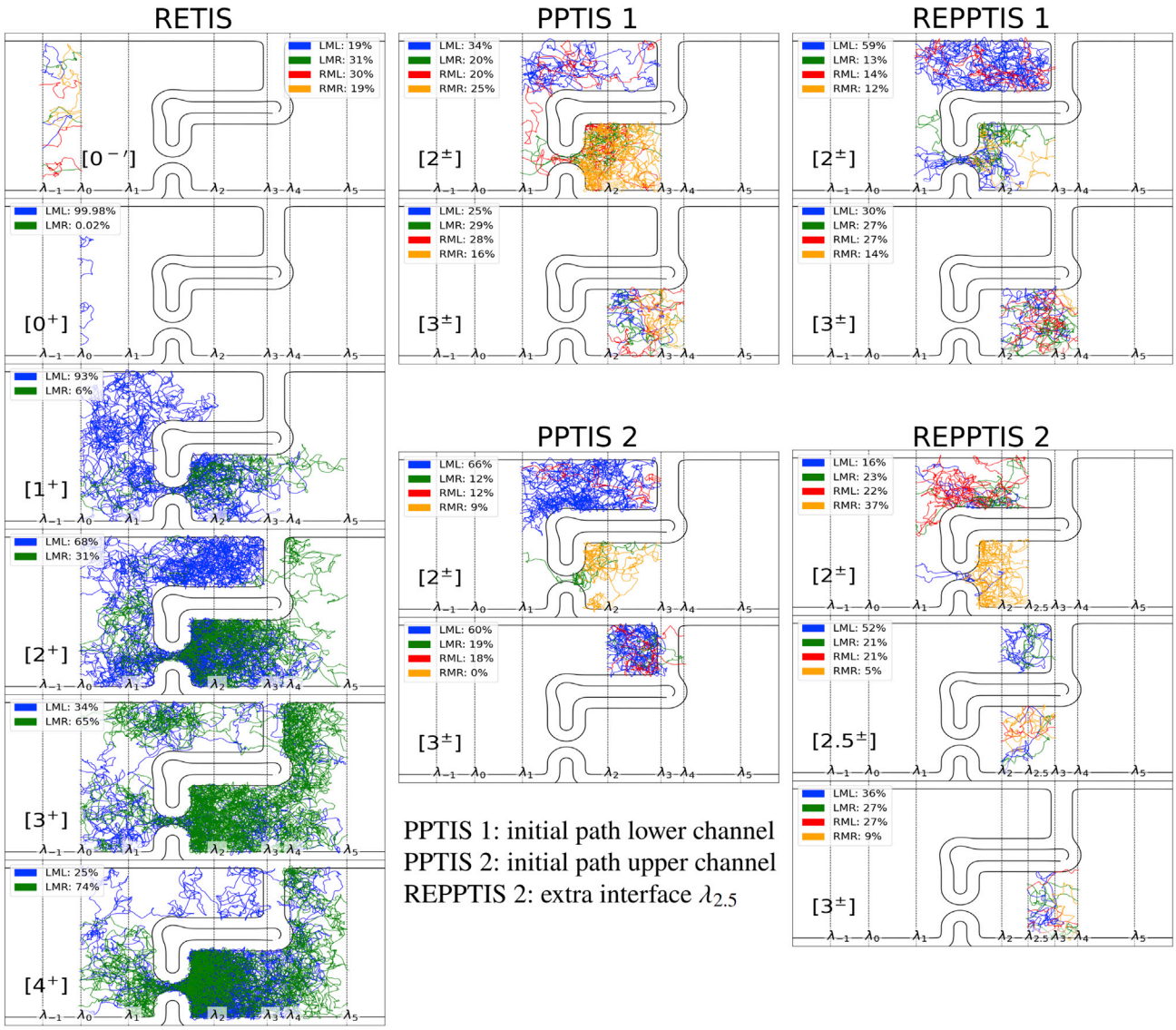

FIGURE 4 Example paths of each simulation. The paths are colored according to the four possible path types, which are determined by the interfaces where the path begins and ends. For example, if a path of the $[i^{\pm}]$ starts at interface λ_{i-1} and ends at interface λ_{i+1}, it is labeled an LMR path as it started from the left (L) of λ_i and ended at the right (R) of λ_i. The four possibilities are LML paths (*blue*), LMR paths (*green*), RML paths (*red*), and RMR paths (*orange*). The weight of each path type is indicated in percentages. For each ensemble, 10 paths are randomly selected, respecting the weight of the path types. For example, of the 10 paths in the $[2^{\pm}]$ PPTIS 1 ensemble, 3 are LML (34%), 2 are LMR (20%), 2 are RML (20%), and 3 are RMR (25%). To see this figure in color, go online.

in $[3^{\pm}]$, as if it had tunneled through the wall. In other words, the particle "forgets" its passage through the flippers. A too harsh reduction of memory can thus lead to an overestimate of the permeability. For REPPTIS 1, no such tunneling occurs between $[2^{\pm}]$ and $[3^{\pm}]$, because λ_3 is located on the rising edge of the energetic barrier. Surprisingly, the REPPTIS 2 crossing probability decreases at the end, resulting in a total crossing probability that lies close to RETIS. This is, however, a lucky cancellation of errors as tunneling also happens from right to left. The paths of RETIS and REPPTIS 1 have a small probability of recrossing the energetic or entropic barriers, while the reverse tunneling in REPPTIS 2 makes this more likely, which results in a decrease of the global crossing probability.

Permeation of ibuprofen drug molecule

Whereas the maze system was built to showcase the role of memory, we now study an application that is more representative for a typical membrane permeability simulation. Passive permeability through (lipid) membranes is of vital importance for drug design, as it gives insight to the timescale at which drugs transit the membrane for a given concentration gradient (6,52). The nonsteroidal anti-inflammatory

drug ibuprofen has to cross several membranes before realizing its inhibitory effect on the cyclooxygenase enzymes COX-1 and COX-2 (53,54). Path sampling is now used to investigate the permeation of ibuprofen through a dioleoylphosphatidylcholine (DOPC) membrane. The presence of metastable states combined with an orthogonal degree of freedom will put REPPTIS to the test.

Assume z is the center-of-mass distance (in unit nanometers) of ibuprofen to the bilayer midplane, and θ is the dihedral angle determining the OH orientation in the carboxyl group of ibuprofen. The free energy profile $F(z,\theta)$ of ibuprofen in a DOPC bilayer is shown in Fig. 5 *A*, which was recreated from data in (55). Details of the implementation can be found in the supporting material. The two stable OH bond conformations are *cis* ($\theta \approx 0$) and *trans* ($\theta \approx \pi$), which are visualized in Fig. 5 *B*. The free energy profile contains minima in each leaflet ($z \in [-1.5, -1]$ and $z \in [1, 1.5]$), such that a full transit across the bilayer consists of at least two successive rare events. This means that RETIS is no viable option to study the full permeation event, as the paths would get stuck in the metastable states, resulting in extremely long paths. The memory reduction in REPPTIS greatly reduces the pathlengths and enables the study of the full permeation using a single simulation.

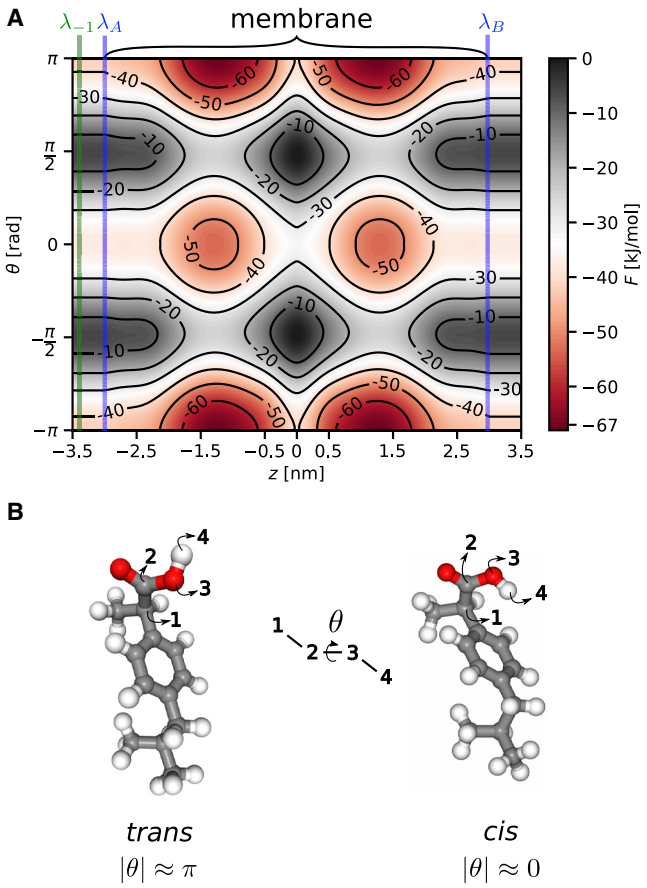

FIGURE 5 (*A*) Two-dimensional free energy profile $F(z,\theta)$ of ibuprofen in a DOPC bilayer. F is periodic in θ with period 2π. The regions $\theta \approx 0$ and $|\theta| \approx \pi$ are the *cis* and *trans* configurations, respectively. The membrane is located in $z \in [-3, 3]$, while $z < -3$ and $z > 3$ represent the water phases near each leaflet. The RETIS simulation to calculate P_{entr} uses the λ_{-1} interface (*green vertical line*). The simulation domains for all other RE(PP)TIS simulations lie in between the λ_A and λ_B interfaces (*blue lines*) of the full permeation REPPTIS simulation. (*B*) Ibuprofen in the *cis* and *trans* configurations. The atoms that define the dihedral angle θ of the hydroxyl hydrogen of the carboxyl group are annotated with arrows. To see this figure in color, go online.

Permeation of ibuprofen through the DOPC bilayer is characterized by three steps, i.e., entering the membrane, hopping over an internal barrier, and escaping from the membrane. Starting from the water phase in $z < -3$, ibuprofen *enters* the energy minimum around $z \in [-1.5, -1.0]$ in the first leaflet. Given that ibuprofen crosses $z = -3$ to the right, the molecule has a crossing probability denoted by P_{entr} to enter into this stable region. This probability is not 1, as friction by the membrane molecules can let the molecule return to -3, rather than fully entering. Next, ibuprofen must overcome the *internal* barrier between the leaflets to reach the second energy minimum $z \in [1, 1.5]$. The corresponding crossing probability over the internal barrier is denoted P_{int}. Finally, ibuprofen needs to *escape* from the second stable region and reach the water phase ($z > 3$). This crossing probability is denoted P_{esc}.

These characteristic crossing probabilities P_{entr}, P_{int}, and P_{esc} are calculated using RETIS and REPPTIS (simulation details in supporting material), and are given in Table 2. Each simulation was run twice, where the initial path was either in the *cis* or *trans* configuration. As it was verified that transitions between these configurations happened in all of the ensembles, the data of both runs were merged.

As the paths would become too long to simulate a full transit with RETIS, the three characteristic crossing probabilities were used in a Markov model to estimate the full transit probability P_{trans} from $z = -3$ to $z = 3$. Let $k_{\text{int}} = f_{\text{int}} P_{\text{int}}$ and $k_{\text{esc}} = f_{\text{esc}} P_{\text{esc}}$ be the internal and escape rates, respectively, where the fluxes f_{int} and f_{esc} are part of the RETIS simulation output. As shown in the supporting material, the transit probability is approximated by $P_{\text{trans}} \approx (P_{\text{entr}} k_{\text{int}})/(k_{\text{esc}} + 2k_{\text{int}})$. In contrast to RETIS, REPPTIS is capable of calculating P_{trans} of the full membrane transit using a single simulation. Both the REPPTIS and the approximate Markov RETIS values of P_{trans} are given in Table 2.

TABLE 2 Characteristic crossing probabilities of ibuprofen permeation through a phospholipid bilayer

Simulation	P_{entr} [10^{-2}]	P_{int} [10^{-6}]	P_{esc} [10^{-6}]	P_{trans} [10^{-3}]
RETIS	17 (±7%)	1.2 (±11%)	2.3 (±8%)	5.4 (±23%)
REPPTIS		1.1 (±8%)	2.2 (±5%)	6.1 (±7%)

P_{trans} is the crossing probability of a full membrane transit: the REPPTIS value is from a simulation, while the RETIS value is an estimate based on a simple Markov model. Reported errors are standard errors based on block averaging.

The RETIS and REPPTIS simulations result in statistically equivalent crossing probabilities for both the internal and escape transitions. From the entrance RETIS simulation, the factor $(\xi\Delta z)/\tau_{\mathrm{ref},[0^-{}']} = (5.0 \pm 1\%) \times 10^{-2}$ nm/ps is obtained, which enters the permeability equation (Eq. 8). Using the Markov model with the characteristic crossing probabilities of the RETIS simulations, the permeability of ibuprofen becomes $(27 \pm 23\%)$ cm/s. Using P_{trans} of the full permeation REPPTIS simulation, the permeability of ibuprofen is estimated to be $(30 \pm 7\%)$ cm/s. This value, based on the two-dimensional $F(z, \theta)$ profile at 303 K of (55), is in reasonable agreement with the ibuprofen permeability (92 ± 6) cm/s through dipalmitoylphosphatidylcholine at 323 K as obtained from MD simulations and the inhomogeneous solubility-diffusion model (56).

CONCLUSION

In this article we first reviewed the recently developed theoretical framework for calculating permeability coefficients using the RETIS methodology. The approach requires a slight modification of the $[0^-]$ path ensemble to the $[0^{-\prime}]$ ensemble, which describes the paths at the left side of λ_A. The RETIS-based permeability can be computed with exponential reduction in time compared with standard MD, while it still gives exactly the same result without introducing any approximation. The mathematical formulation of microscopic permeability in terms of RETIS properties has the advantage that recent algorithmic developments in the RETIS method can directly be applied, such as the recently developed MC moves for generating new paths more efficiently (17,30,31) and the nonsynchronous replica exchange approach (32).

However, if the individual transition paths themselves are long, it may be wise to give up some of the method's exactness for the sake of obtaining shorter paths. This idea underlies the PPTIS method in which the statistics of long transition paths is obtained via paths with much shorter range using a memory loss assumption. Still, some memory is retained in the conditional local crossing probabilities that are computed. In this article, we combined the PPTIS method with replica exchange into a new implementation, coined the REPPTIS method. We applied PPTIS and REPPTIS on a didactic model and on the permeation of ibuprofen based on a realistic free energy surface. The results showed the importance of both replica exchange and memory, as simulations without them gave wrong permeability estimates.

There are several interesting opportunities to improve the REPPTIS method further. Note that the extension of paths by means of MD in a swapping move could yield additional information that adds back in some of the lost memory. Before the extended trajectories are trimmed to fit the boundaries of the new path ensemble, these extensions provide continuous trajectories that go beyond the range of three consecutive interfaces. Using the information of untrimmed trajectories might be exploited in future variants of the REPPTIS method since it could solve the conflicting benefits of having interfaces close enough for efficiency and far apart for accuracy. Moreover, the time information is not yet exploited by TIS-based methods. For instance, the PPTIS crossing probabilities relate to the chance that a specific interface is crossed before another irrespective how long it takes. Another future development that we want to achieve is the inclusion of time durations in the statistical description of the crossing probabilities, as is done in milestoning, to compute (conditional) mean first passage times and diffusion coefficients. Note that other milestone variations such as the use of multidimensional interface networks via, e.g., Voronoi cells (57), can in principle be applied within a REPPTIS framework as well. We can therefore conclude that REPPTIS is a promising method to enable permeation simulations with high efficiency and accuracy that might not be easily achieved by any other method.

SUPPORTING MATERIAL

Supporting material can be found online at https://doi.org/10.1016/j.bpj.2023.02.021.

AUTHOR CONTRIBUTIONS

A.G. and T.S.v.E. designed the research. W.V. and D.Z. carried out all simulations. W.V., T.S.v.E., and A.G. analyzed the data. W.V., T.S.v.E., and A.G. wrote the article with input from all authors.

ACKNOWLEDGMENTS

The computational resources (Stevin Supercomputer Infrastructure) and services used in this work were provided by the VSC (Flemish Supercomputer Center), funded by Ghent University, FWO and the Flemish Government – department EWI. We acknowledge funding of the FWO (project G002520N and project G094023N) and the Research Council of Norway (project Theolight, grant no. 275506).

DECLARATION OF INTERESTS

The authors declare no competing interests.

REFERENCES

1. Yang, N. J., and M. J. Hinner. 2015. Getting across the cell membrane: an overview for small molecules, peptides, and proteins. *In* Site-Specific Protein Labeling: Methods and Protocols. A. Gautier and M. J. Hinner, eds Springer, pp. 29–53.
2. Awoonor-Williams, E., and C. N. Rowley. 2016. Molecular simulation of nonfacilitated membrane permeation. *Biochim. Biophys. Acta.* 1858:1672–1687.
3. Shinoda, W. 2016. Permeability across lipid membranes. *Biochim. Biophys. Acta.* 1858:2254–2265.

4. Bennion, B. J., N. A. Be, …, T. S. Carpenter. 2017. Predicting a drug's membrane permeability: a computational model validated with in vitro permeability assay data. *J. Phys. Chem. B.* 121:5228–5237.
5. Hannesschlaeger, C., A. Horner, and P. Pohl. 2019. Intrinsic membrane permeability to small molecules. *Chem. Rev.* 119:5922–5953.
6. Menichetti, R., K. H. Kanekal, and T. Bereau. 2019. Drug-membrane permeability across chemical space. *ACS Cent. Sci.* 5:290–298.
7. Levental, I., and E. Lyman. 2023. Regulation of membrane protein structure and function by their lipid nano-environment. *Nat. Rev. Mol. Cell Biol.* 24:79.
8. Dotson, R. J., C. R. Smith, …, S. C. Pias. 2017. Influence of cholesterol on the oxygen permeability of membranes: insight from atomistic simulations. *Biophys. J.* 112:2336–2347.
9. Venable, R. M., A. Krämer, and R. W. Pastor. 2019. Molecular dynamics simulations of membrane permeability. *Chem. Rev.* 119: 5954–5997.
10. Davoudi, S., and A. Ghysels. 2021. Sampling efficiency of the counting method for permeability calculations estimated with the inhomogeneous solubility–diffusion model. *J. Chem. Phys.* 154, 054106.
11. Marrink, S. J., and H. J. C. Berendsen. 1994. Simulation of water transport through a lipid membrane. *J. Phys. Chem.* 98:4155–4168.
12. De Vos, O., R. M. Venable, …, A. Ghysels. 2018. Membrane permeability: characteristic times and lengths for oxygen and a simulation-based test of the inhomogeneous solubility-diffusion model. *J. Chem. Theory Comput.* 14:3811–3824.
13. Ghysels, A., A. Krämer, …, R. W. Pastor. 2019. Permeability of membranes in the liquid ordered and liquid disordered phases. *Nat. Commun.* 10:5616.
14. Torrie, G., and J. Valleau. 1977. Nonphysical sampling distributions in Monte Carlo free-energy estimation: umbrella samping. *J. Comput. Phys.* 23:187–199.
15. Darve, E., and A. Pohorille. 2001. Calculating free energies using average force. *J. Chem. Phys.* 115:9169–9183.
16. Comer, J., J. C. Gumbart, …, C. Chipot. 2015. The adaptive biasing force method: everything you always wanted to know but were afraid to ask. *J. Phys. Chem. B.* 119:1129–1151.
17. Ghysels, A., S. Roet, …, T. S. van Erp. 2021. Exact non-Markovian permeability from rare event simulations. *Phys. Rev. Res.* 3, 033068.
18. van Erp, T. S., D. Moroni, and P. G. Bolhuis. 2003. A novel path sampling method for the calculation of rate constants. *J. Chem. Phys.* 118:7762–7774.
19. Faradjian, A. K., and R. Elber. 2004. Computing time scales from reaction coordinates by milestoning. *J. Chem. Phys.* 120:10880–10889.
20. Allen, R. J., P. B. Warren, and P. R. ten Wolde. 2005. Sampling rare switching events in biochemical networks. *Phys. Rev. Lett.* 94, 018104.
21. Metropolis, N., A. W. Rosenbluth, …, E. Teller. 1953. Equation of state calculations by fast computing machines. *J. Chem. Phys.* 21: 1087–1092.
22. van Erp, T. 2012. Dynamical rare event simulation techniques for equilibrium and nonequilibrium systems. *Adv. Chem. Phys.* 151:27.
23. Moroni, D., P. G. Bolhuis, and T. S. van Erp. 2004. Rate constant for diffusive processes by partial path sampling. *J. Chem. Phys.* 120:4055–4065.
24. Vanden-Eijnden, E., M. Venturoli, …, R. Elber. 2008. On the assumptions underlying milestoning. *J. Chem. Phys.* 129, 174102.
25. Cardenas, A. E., and R. Elber. 2013. Computational study of peptide permeation through membrane: searching for hidden slow variables. *Mol. Phys.* 111:3565–3578.
26. Cardenas, A. E., and R. Elber. 2014. Modeling kinetics and equilibrium of membranes with fields: milestoning analysis and implication to permeation. *J. Chem. Phys.* 141, 054101.
27. Fathizadeh, A., and R. Elber. 2019. Ion permeation through a phospholipid membrane: transition state, path splitting, and calculation of permeability. *J. Chem. Theory Comput.* 15:720–730.
28. Votapka, L. W., C. T. Lee, and R. E. Amaro. 2016. Two relations to estimate membrane permeability using milestoning. *J. Phys. Chem. B.* 120:8606–8616.
29. Riccardi, E., A. Krämer, …, A. Ghysels. 2021. Permeation rates of oxygen transport through POPC membrane using replica exchange transition interface sampling. *J. Phys. Chem. B.* 125:193–201.
30. Riccardi, E., O. Dahlen, and T. S. van Erp. 2017. Fast decorrelating Monte Carlo moves for efficient path sampling. *J. Phys. Chem. Lett.* 8:4456–4460.
31. Zhang, D. T., E. Riccardi, and T. S. van Erp. 2023. Path sampling with sub-trajectory moves. *J. Chem. Phys.* 158:024113.
32. Roet, S., D. T. Zhang, and T. S. van Erp. 2022. Exchanging replicas with unequal cost, infinitely and permanently. *J. Phys. Chem. A.* 126:8878–8886.
33. Davoudi, S., and A. Ghysels. 2023. Defining permeability of curved membranes in molecular dynamics simulations. *Biophys. J.* 122:1–10. https://doi.org/10.1016/j.bpj.2022.11.028.
34. Dellago, C., P. G. Bolhuis, and P. L. Geissler. 2002. Transition path sampling. *Adv. Chem. Phys.* 123:1.
35. Hummer, G. 2005. Position-dependent diffusion coefficients and free energies from Bayesian analysis of equilibrium and replica molecular dynamics simulations. *New J. Phys.* 7:34.
36. Ghysels, A., R. M. Venable, …, G. Hummer. 2017. Position-dependent diffusion tensors in anisotropic media from simulation: oxygen transport in and through membranes. *J. Chem. Theory Comput.* 13:2962–2976.
37. Krämer, A., A. Ghysels, …, R. W. Pastor. 2020. Membrane permeability of small molecules from unbiased molecular dynamics simulations. *J. Chem. Phys.* 153, 124107.
38. Dellago, C., P. G. Bolhuis, and D. Chandler. 1998. Efficient transition path sampling: application to Lennard-Jones cluster rearrangements. *J. Chem. Phys.* 108:9236–9245.
39. Hastings, W. 1970. Monte-Carlo sampling methhods using Markov chains and their applications. *Biometrika.* 57:97.
40. van Erp, T. S. 2007. Reaction rate calculation by parallel path swapping. *Phys. Rev. Lett.* 98, 268301.
41. Cabriolu, R., K. M. Skjelbred Refsnes, …, T. S. van Erp. 2017. Foundations and latest advances in replica exchange transition interface sampling. *J. Chem. Phys.* 147, 152722.
42. Dellago, C., P. G. Bolhuis, …, D. Chandler. 1998. Transition path sampling and the calculation of the rate constant. *J. Chem. Phys.* 108:1964–1977.
43. van Erp, T. S., M. Moqadam, …, A. Lervik. 2016. Analyzing complex reaction mechanisms using path sampling. *J. Chem. Theory Comput.* 12:5398–5410.
44. Plattner, N., J. D. Doll, …, J. E. Gubernatis. 2011. An infinite swapping approach to the rare-event sampling problem. *J. Chem. Phys.* 135, 134111.
45. Plattner, N., J. D. Doll, and M. Meuwly. 2013. Overcoming the rare event sampling problem in biological systems with infinite swapping. *J. Chem. Theory Comput.* 9:4215–4224.
46. Yu, T.-Q., J. Lu, …, E. Vanden-Eijnden. 2016. Multiscale implementation of infinite-swap replica exchange molecular dynamics. *Proc. Natl. Acad. Sci. USA.* 113:11744–11749.
47. Lu, J., and E. Vanden-Eijnden. 2019. Methodological and computational aspects of parallel tempering methods in the infinite swapping limit. *J. Stat. Phys.* 174:715–733.

48. van Erp, T. S., and P. G. Bolhuis. 2005. Elaborating transition interface sampling methods. *J. Comput. Phys.* 205:157–181.

49. Moqadam, M., A. Lervik, …, T. S. van Erp. 2018. Local initiation conditions for water autoionization. *Proc. Natl. Acad. Sci. USA.* 115:E4569–E4576.

50. Lervik, A., E. Riccardi, and T. S. van Erp. 2017. PyRETIS: a well-done, medium-sized python library for rare events. *J. Comput. Chem.* 38:2439–2451.

51. Riccardi, E., A. Lervik, …, T. S. van Erp. 2020. PyRETIS 2: an improbability drive for rare events. *J. Comput. Chem.* 41:370–377.

52. Di, L., P. Artursson, …, K. Sugano. 2020. The critical role of passive permeability in designing successful drugs. *ChemMedChem.* 15: 1862–1874.

53. Choi, S.-H., S. Aid, and F. Bosetti. 2009. The distinct roles of cyclooxygenase-1 and-2 in neuroinflammation: implications for translational research. *Trends Pharmacol. Sci.* 30:174–181.

54. Novakova, I., E.-A. Subileau, …, W. Neuhaus. 2014. Transport rankings of non-steroidal antiinflammatory drugs across blood-brain barrier in vitro models. *PLoS One.* 9, e86806.

55. Jämbeck, J. P. M., and A. P. Lyubartsev. 2013. Exploring the free energy landscape of solutes embedded in lipid bilayers. *J. Phys. Chem. Lett.* 4:1781–1787.

56. Boggara, M. B., and R. Krishnamoorti. 2010. Partitioning of nonsteroidal antiinflammatory drugs in lipid membranes: a molecular dynamics simulation study. *Biophys. J.* 98:586–595.

57. Vanden-Eijnden, E., and M. Venturoli. 2009. Markovian milestoning with Voronoi tessellations. *J. Chem. Phys.* 130, 194101.

Biophysical Journal, Volume *122*

Supplemental information

Path sampling with memory reduction and replica exchange to reach long permeation timescales

Wouter Vervust, Daniel T. Zhang, Titus S. van Erp, and An Ghysels

SUPPLEMENTARY INFORMATION

Path sampling with memory reduction and replica exchange to reach long permeation timescales

Wouter Vervust,[1] Daniel T. Zhang,[2] Titus S. van Erp,[2] and An Ghysels[1]

[1)] *IBiTech - BioMMedA research group, Faculty of Engineering and Architecture, Ghent University, Corneel Heymanslaan 10, Block B (entrance 36), 9000 Gent, Belgium*

[2)] *Department of Chemistry, Norwegian University of Science and Technology, NO-7491 Trondheim, Norway*

I. THE 2D MAZE

A. Construction of the maze

The maze is first drawn as a pixel map, as shown in Fig. S1a. Maze pixels are labeled as a horizontal wall, a vertical wall, or as both horizontal and vertical walls thus creating a corner.

The walls of the maze generate repulsive forces acting on the Langevin particle. Consider for instance the vertical wall in Fig. S1b with wall thickness $2d_w$. The distance d is defined as the distance from the Langevin particle to the center of the wall. When d is large, beyond a cutoff value D, the particle experiences no interaction with the wall. When the particle approaches the wall and $d < D$, the wall exerts a repulsive force on the particle. On top of a wall when $d < d_w$, the Langevin particle has a constant potential energy and does not experience any force either. The force $F_{\text{wall}}(d)$ scales as a Gaussian function and continuously approaches 0 at $d = d_w$. For $d_w < d \leq D$, the force is given by

$$F_{\text{wall}}(d) = \frac{a}{c^2}(d - d_w)e^{-d^2/(2c^2)}, \tag{1}$$

while the force exerted by the wall is 0 elsewhere. The parameter c is a measure for the steepness of the wall's slope, and a is a measure for the height of the wall. The value of the cutoff distance D should be taken large enough such that the force becomes negligible at $d = D$. In Fig. S1a, black pixels represent very high walls with $a = 500$, while the red pixels represent a lower wall with $a = 25$. The steepness parameter was set to $c = \delta$, the wall thickness to $2d_w = \delta$, and the cutoff value $D = 4\delta$, where $\delta = 1/59$ is the pixel width in the maze design with 59×59 pixels covering an area of 1 by 1.

When the particle is within the cutoff D of two or more walls, the particle only feels the superposition of the closest horizontal and closest vertical wall. Consequently, the potential energy function remains continuous and continuously differentiable in the vicinity of corners, which are characterized as both a vertical and horizontal wall.

In our implementation of the maze potential, the cutoff D is exploited to reduce the CPU-time of the energy and force calculation. Assume the the Langevin particle is positioned at (x_p, y_p). First, the discrete pixel indices (i_p, j_p) of the particle are determined. Then, the detection area is set to a square grid of $(2n_D + 1) \times (2n_D + 1)$ pixels centered around the particle's pixel (i_p, j_p), with $n_D = D/\delta = 4$ in this paper. Only the walls in these

$(2n_D + 1)^2$ pixels are examined to determine the interaction with the particle, which keeps the simulation time-efficient even for large mazes.

The Langevin particle dynamics were integrated with the PyRETIS internal engine. In a Lennard-Jones type of unit system, based on argon[1], the following parameters were used: particle mass $m = 1$, temperature $T = 0.07$, friction coefficient $\gamma = 25$, and integration timestep $\Delta t = 0.01$. The interfaces are placed at $\lambda_A = 0.2$, 0.325, 0.55, 0.69, 0.75, and $0.90 = \lambda_b$.

For completeness, we report the two other factors in Eq. 7 of the main text to be $\xi = 0.48$ ($\pm 1.3\%$) and $\tau_{\mathrm{ref},[0^-\prime]}/\Delta z = 4.86$ ($\pm 0.7\%$).

The simulation input files, together with the maze potential code, can be found on github: WouterWV/pathsampling_toymodels.

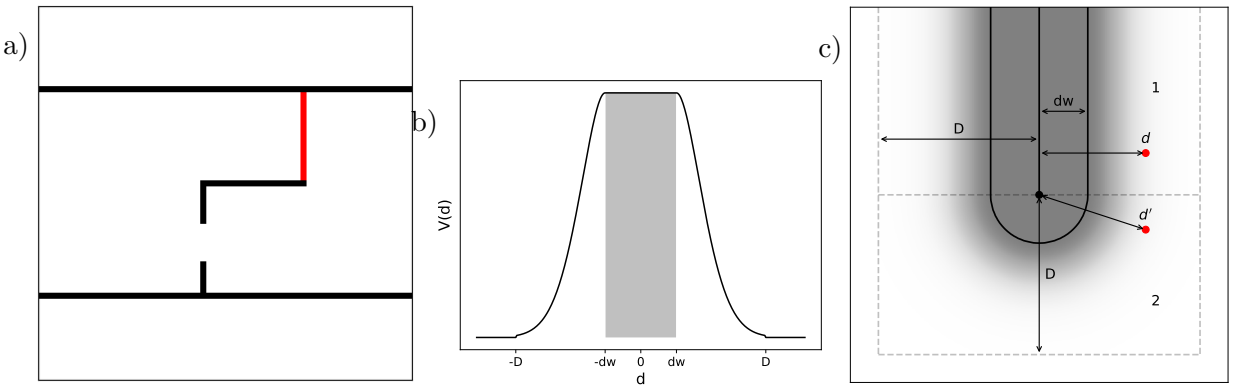

FIG. S1: (a) Pixel map (59 by 59 pixels) used to construct the maze potential in an area of 1 by 1. The red pixels form a lower energetic barrier in the upper channel, while the black pixels are high walls that are nearly impenetrable. (b) Wall potential corresponding to force in Eq. 1. Particles within a distance D of the wall center feel a force exerted by the wall. The top of the wall (distance $< d_w$) is a flat potential. (c) Heat-map of the potential of a vertical wall. A horizontal force is felt in the upper area (area 1). A particle (red) with distance d from the wall center is drawn. A radial force is felt in the lower area (area 2). The magnitude of the force in area 2 is determined by the distance d' to the 'wall center edge'. Particles do not feel a force beyond the cutoff D.

B. 2D histograms of (RE)PPTIS path ensembles

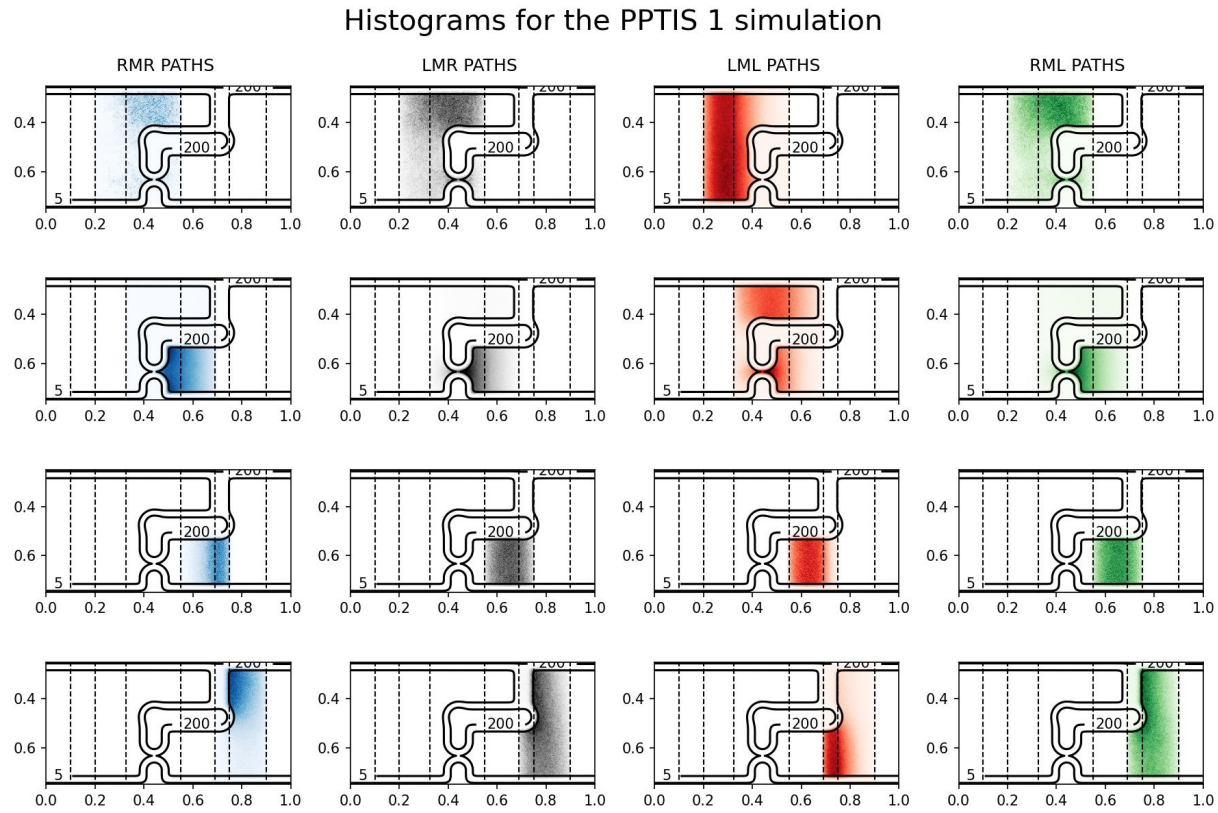

FIG. S2: Visualization of the different path types in each ensemble, for the PPTIS 1 simulation. For each path type, and for each ensemble, the phasepoints of all the trajectories were histogrammed and visualized using a heatmap. The rows from top to bottom correspond with ensembles $[1^{\pm}]$, $[2^{\pm}]$, $[3^{\pm}]$ and $[4^{\pm}]$, and the columns left to right correspond with path types RMR, LMR, LML and RML. The dashed vertical lines in each plot represent the interfaces $(\lambda_{-1}, \lambda_A, \ldots, \lambda_B)$

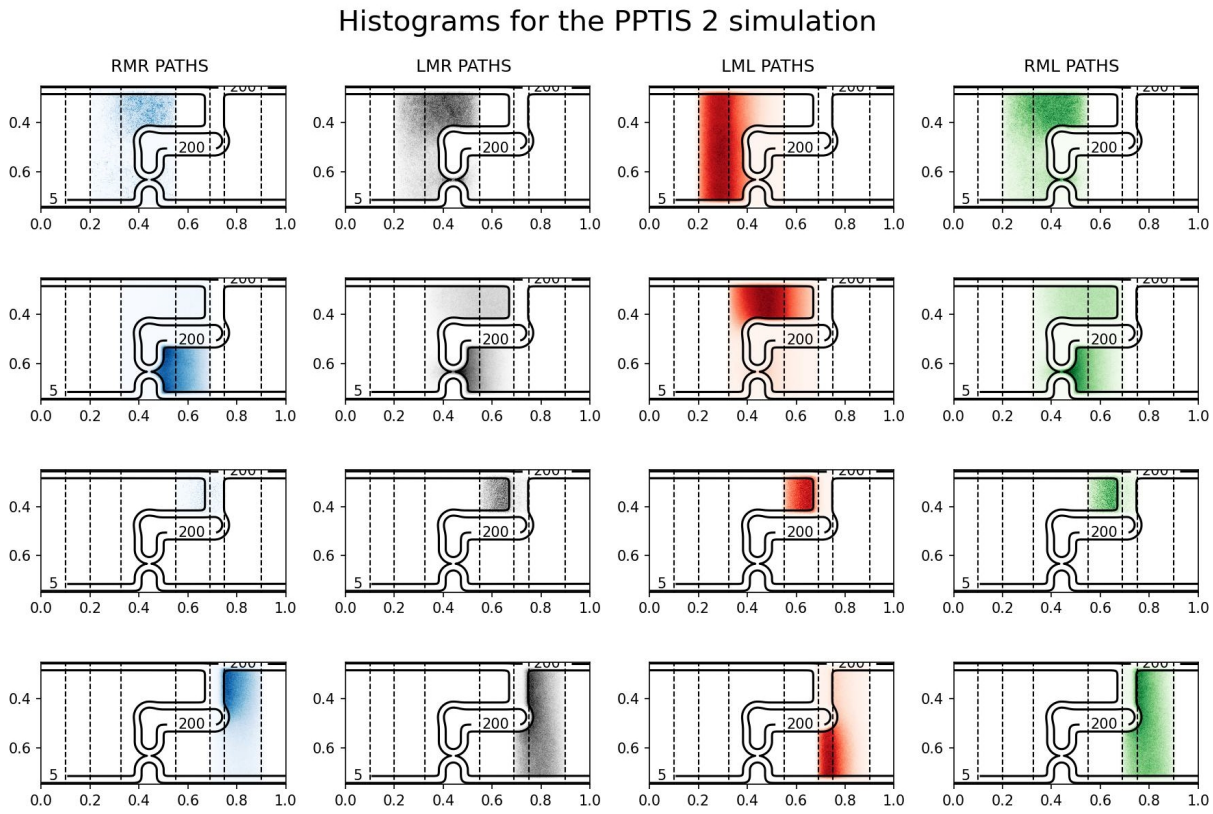

FIG. S3: Same as Fig. S2, for the PPTIS 2 simulation.

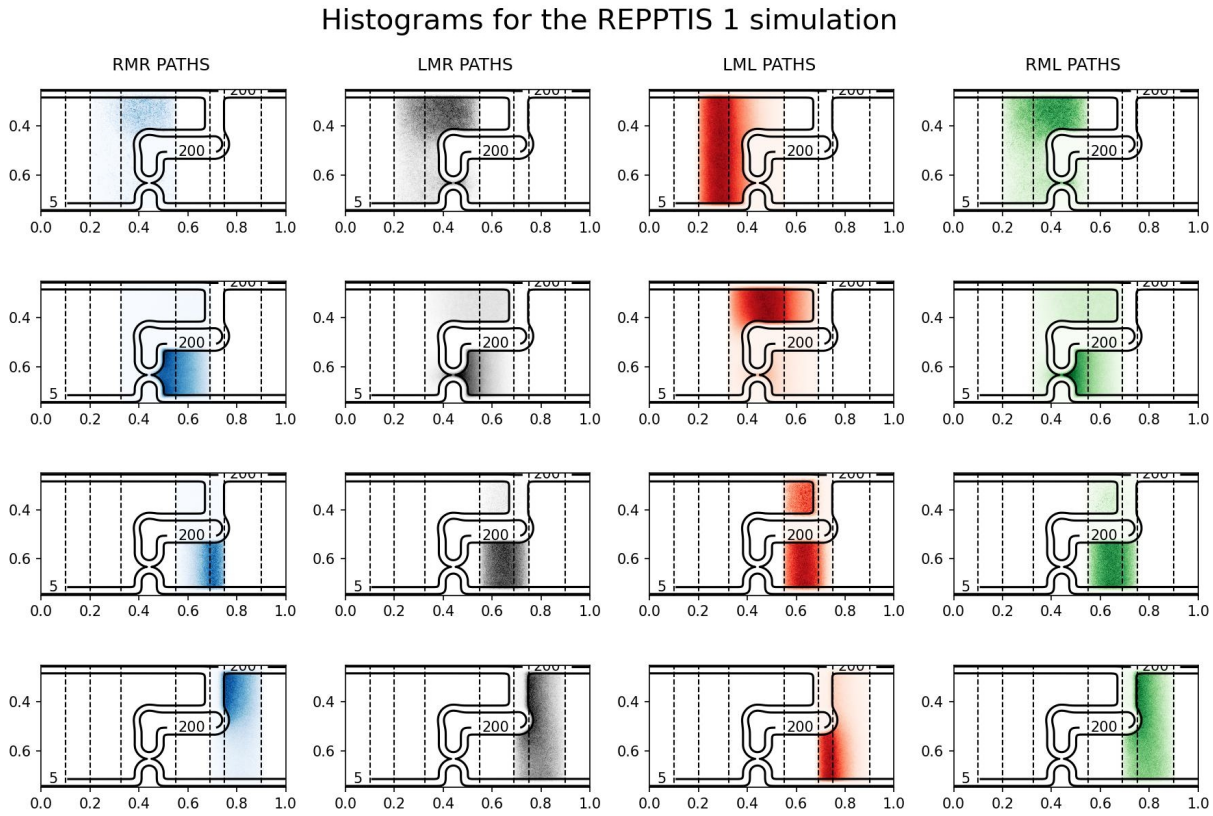

FIG. S4: Same as Fig. S2, for the REPPTIS 1 simulation.

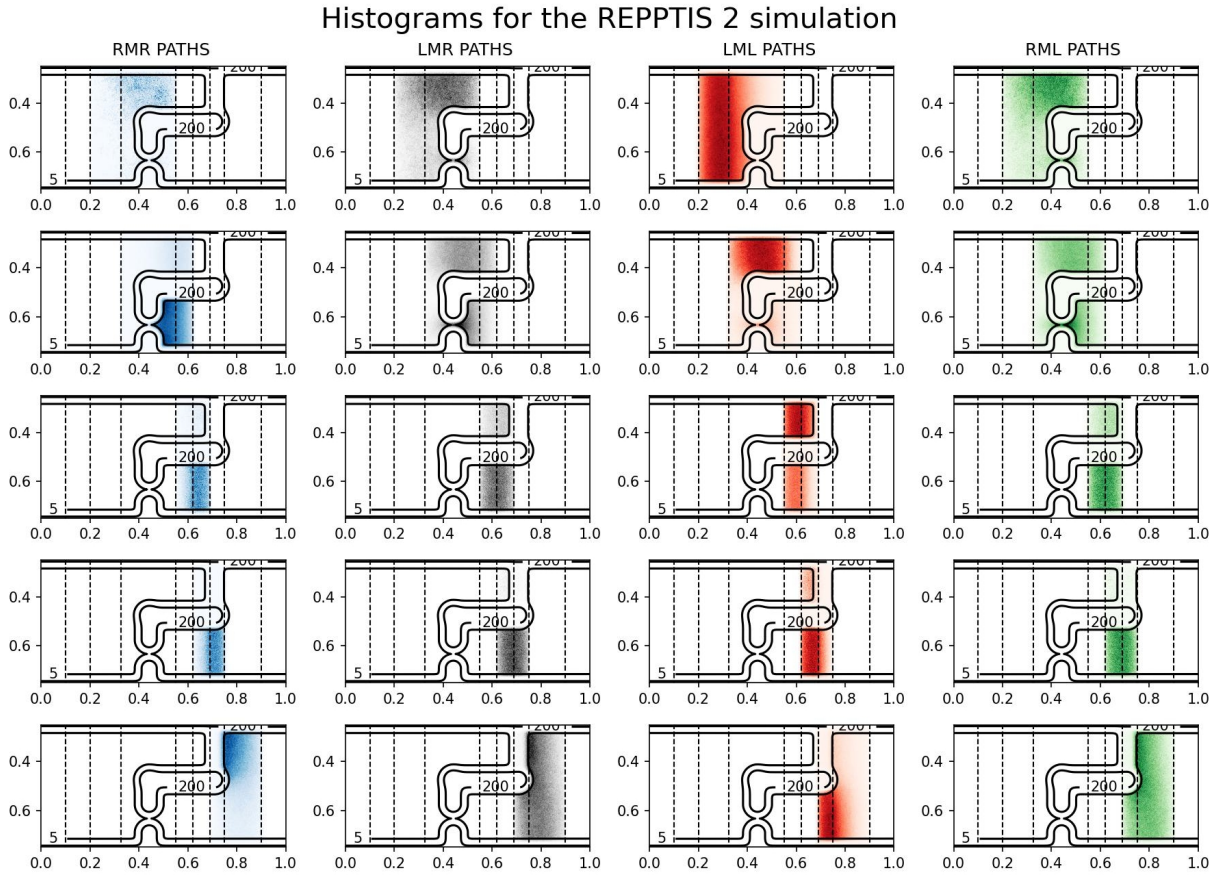

FIG. S5: Same as Fig. S2, for the REPPTIS 2 simulation. An extra row is included for REPPTIS 2, due to the extra interface $\lambda_{2.5}$. The rows from top to bottom correspond with ensembles $[1^{\pm}]$, $[2^{\pm}]$, $[2.5^{\pm}]$, $[3^{\pm}]$ and $[4^{\pm}]$, and the columns left to right correspond with path types RMR, LMR, LML and RML.

.

II. IBUPROFEN PERMEATION

A. Reconstructing the free energy 2D surface of ibuprofen

The two-dimensional free energy profile $F_{\text{true}}(z, \theta)$ of ibuprofen in a DOPC bilayer is reported by Jambeck et al. in Fig. 2a of Ref. 2, as obtained from all-atom molecular dynamics simulations. The authors also report one-dimensional slices of the profile as a function of z for the *cis* and *trans* configurations, and the free energy profile as a function of θ in water and hexadecane. Tracing these profiles and approximating them with analytical functions allowed us to reconstruct a free energy profile $F(z, \theta)$ resembling their $F_{\text{true}}(z, \theta)$ profile. We will now provide the details how this was done.

One-dimensional slices $F^{cis}_{\text{true}}(z) \equiv F_{\text{true}}(z, \theta = 0)$ and $F^{trans}_{\text{true}} \equiv F_{\text{true}}(z, \theta = \pi)$ are provided in Fig. 2b of Ref. 2. First, these profiles were extracted from the figure using in-house code, which resulted in 716 equidistant sample points $\mathcal{S}_M = \{z_i, F^s_i\}_{i=1\ldots716}$ ranging from 0 to 3.5 nm, with sample spacing $\Delta z_s = 3.5\,\text{nm}/715$. Next, two artificial extensions of the grid were added to the left and the right of this interval. To the left, 50 artificial sample points $\mathcal{S}_L = \{z_1 - i\Delta z_s, F^s_1\}_{i=50\ldots1}$ were added, such that oscillations introduced by the polynomial fit (Runge's phenomenom) are suppressed near $z \approx 0$. The same was done on the right, where 50 artificial sample points $\mathcal{S}_R = \{z_{716} + i\Delta z_s, F^s_{716}\}_{i=1\ldots50}$ were added. Hereafter, a polynomial fit of order 15 was performed to $\mathcal{S} = \mathcal{S}_L \cup \mathcal{S}_M \cup \mathcal{S}_R$. This resulted in the reconstructed profiles $F^{cis}(z) \equiv F(z, \theta = 0)$ and $F^{trans}(z) \equiv F(z, |\theta| = \pi)$, which are shown in Fig. S6a. The regions of the artificial extensions to the left and right are never used in the simulations, as only the domain $z \in [0, 3.4\,\text{nm}]$ is sampled in the PyRETIS path ensembles.

The free energy profiles of ibuprofen in water ($F^{\text{water}}_{\text{true}}(\theta)$) and in n-hexane ($F^{n\text{-hexane}}_{\text{true}}(\theta)$) are provided in Fig. S1 of Ref. 2. These profiles were extracted from the figure using in-house code, resulting in 713 equidistant sample points, with sample spacing $\Delta\theta_s = (2\pi)/712$. A Fourier reconstruction of order 11 was used to reconstruct the profiles from the sample points. As the profile is periodic in θ with period 2π, no Gibbs phenomenom occurs, and no artificial extensions were required. This resulted in the reconstructed profiles $F(z = 0, \theta)$ and $F(z = 3.5\,\text{nm}, \theta)$, which are shown in Fig. S6b.

The free energy profile $F(z, \theta)$ used in our simulations is defined as a linear combination

of the reconstructed one-dimensional profiles

$$F(z,\theta) = F^{cis}(z)\frac{\pi-\theta}{\pi} + F^{trans}(z)\frac{\theta}{\pi} + F^{\text{water}}(\theta)\frac{z}{3.5\,\text{nm}} + F^{n\text{-hexane}}(\theta)\frac{3.5\,\text{nm}-z}{3.5\,\text{nm}}, \qquad (2)$$

for $z \in [0, 3.4\,\text{nm}]$ and $\theta \in [0, \pi]$. Symmetry operations are used to obtain $F(z,\theta)$ for $z \in [-3.4\,\text{nm}, 0]$ and $\theta \notin [0, \pi]$.

The force vector is given by $\left(\frac{\partial F}{\partial z}, \frac{\partial F}{\partial \theta}\right)$. As the reconstructed profiles consist of either polynomials or trigonometric functions, the gradient of Eq. 2 could be computed analytically.

For the water phase region, the reconstruction is ideal, i.e. the original profile describes ibuprofen in water, and in the reconstructed profile it is also positioned in the water phase. For the bilayer interior region, the reconstruction might not be ideal, as n-hexane is possibly a better descriptor of the lipid tail regions $|z| \approx 1$, rather than the midplane region $z = 0$. Nevertheless, the reconstructed profile F more than suffices for the purpose of our simulations.

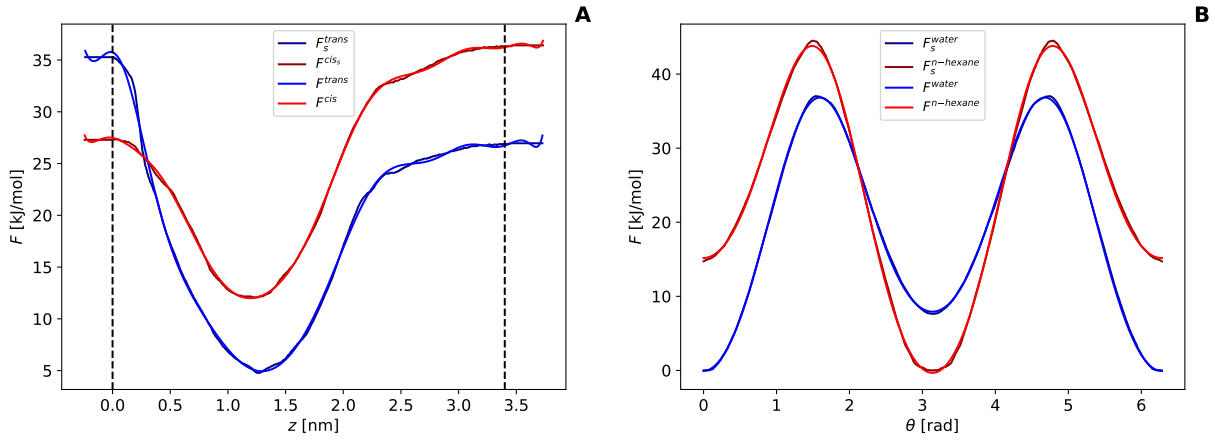

FIG. S6: Reconstructed profiles. For the z-dependent profiles on the left, only the region within the dashed lines is used for the RE(PP)TIS simulations.

B. Langevin dynamics for ibuprofen

The z and θ coordinates of ibuprofen were modeled as two 1D Langevin particles in the PyRETIS code with each their own 'mass'. This mass figures in the kinetic energy term and in the friction term in the Langevin equation. For z, which describes the center-of-mass motion of ibuprofen through the membrane, the associated mass is the total mass of the ibuprofen. For θ, the associated mass is the moment of inertia of the OH bond about the dihedral angle axis, which is the CO bond. In practice, this moment of inertia can be roughly estimated as $m_{\mathrm{H}} d_{\mathrm{OH}}^2$, with m_{H} equal to hydrogen mass, and d_{OH}^2 the average OH bond length. Coriolis effects were neglected, which is acceptable given the friction. Using one 2D Langevin particle would not have worked well here, as PyRETIS assigns one mass to one particle. The mass of ibuprofen, which determines the resistance to the center-of-mass (COM) displacement along z, differs greatly from the inertial moment determining the resistance to rotational displacement along θ, and these masses cannot be approximated by a single value.

The temperature was taken to match the temperature of Ref. 2. A typical friction value of $\gamma = 50\ \mathrm{ps}^{-1}$ was used in the Langevin dynamics which is assumed to be appropriate for aqueous solution.[3] The same friction value was used for z as for θ. GROMACS units (time in ps, length in nm, mass in u, temperature in K) were used to set the Langevin parameters for ibuprofen. The following parameters were used: integration timestep $\Delta t = 0.02\,\mathrm{ps}$, temperature $T = 303\,\mathrm{K}$, friction coefficient $\gamma = 50/\mathrm{ps}$, mass of particle one (z-displacement) $m_{\mathrm{COM}} = 206.31\,\mathrm{u}$, and mass of particle two (θ-displacement) $m_{\mathrm{angle}} = 0.0093\,\mathrm{u}$.

The simulation input files, together with the ibuprofen potential code, can be found on github: WouterWV/pathsampling_toymodels.

C. RE(PP)TIS simulations of ibuprofen

The order parameter λ is the z coordinate. Six simulations were run with PyRETIS:

1. RETIS entrance
2. RETIS internal barrier
3. REPPTIS internal barrier
4. RETIS escape

5. REPPTIS escape
6. REPPTIS full transit

Modeling the full transit is not possible with RETIS because of the two stable states in the leaflet, where trajectories would get trapped. Modeling the entrance was only done with RETIS, because this simulation only needs 3 interfaces and it does not suffer from long trapped paths; hence a REPPTIS simulation would not be that useful.

In practice, two runs were done for each of the six simulations: the simulations were started both from the *cis* and *trans* configuration of ibuprofen. It was verified that all simulations exhibited conformational changes between the *trans* and *cis* conformations, and that these changes occurred in all ensembles. This implies that the two runs are effectively modeling the same system. Therefore, in the reporting of the results, the data of the two runs were combined.

The interfaces used in each of the simulations are given in Tab. S1. REPPTIS uses more interfaces, as both the 'rising' and 'falling' edges of the free energy barrier require interfaces that are separated by $\sim 2k_BT$. RETIS only requires interfaces on the 'rising' edge (and one in stable state B). REPPTIS paths are, however, considerably shorter. The λ_A and λ_B interfaces are matched in RETIS and REPPTIS. For simulation 6, the symmetry of the free energy profile around $z = 0$ was used to (almost) cut the simulation domain in half. Indeed, the interfaces are given by $[-3\,\mathrm{nm}, \ldots, 0, \lambda_b, \lambda_c]$, where the 2 extra interfaces λ_b and λ_c were added such that the $[i^{\pm}]$ with $z = 0$ as middle interface was also sampled. The local crossing probabilities in the $[i^{\pm}]$ ensembles for $z > 0$ can be copied from their symmetric counterpart ensembles in $z < 0$. For run 1, $[7^{\pm}]$ is the PPTIS ensemble with $[\lambda_L, \lambda_M, \lambda_R] = [-0.384\,\mathrm{nm}, 0, 0.384\,\mathrm{nm}]$. The local crossing probabilities of $[(i+N)^{\pm}]$ are given by their symmetric counterpart values in $[(i-N)^{\pm}]$. For example, $p^{\pm}_{[6^{\pm}]} \equiv p^{\mp}_{[8^{\mp}]}$ and $p^{=}_{[5^{\pm}]} \equiv p^{\ddagger}_{[9^{\pm}]}$.

Denote N^i_j as the amount of RE(PP)TIS cycles for run i of simulation j. Then $N^1_1 = 91600$, $N^2_1 = 100000$, $N^1_2 = 24982$, $N^2_2 = 21950$, $N^1_3 = 43101$, $N^2_3 = 45236$, $N^1_4 = 31231$, $N^2_4 = 28966$, $N^1_5 = 100001$, $N^2_5 = 74430$, $N^1_6 = 16506$, and $N^2_6 = 17355$.

The crossing probabilities $P(\lambda_i|\lambda_A)$ for simulations 2, 3, 4 and 5 are given in Fig. S7. REPPTIS and RETIS give statistically identical results.

The crossing probabilities $P(\lambda_i|\lambda_A)$ for simulation 6 are given in Fig. S8. The crossing

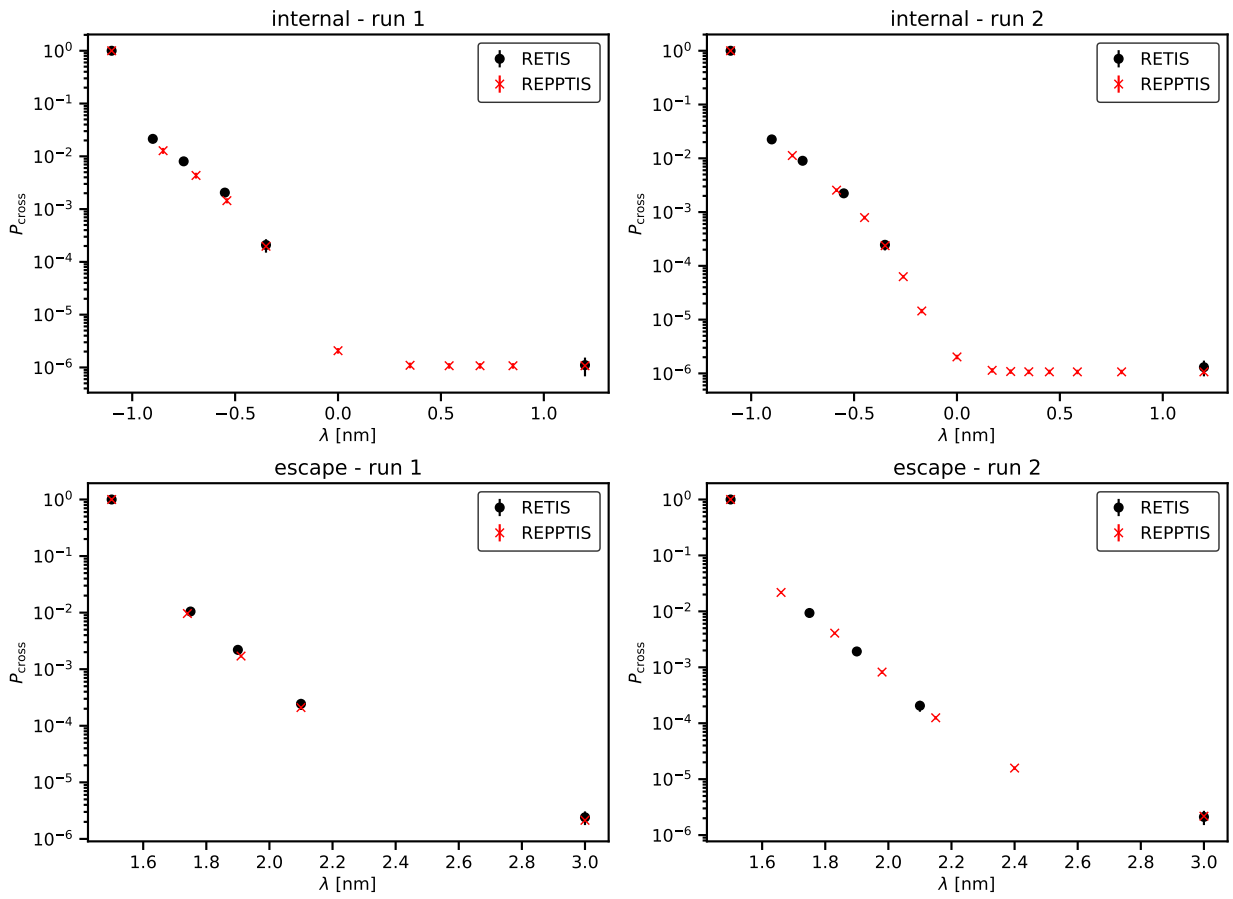

FIG. S7: Crossing probabilities for the internal barrier (top) and the escape (bottom), studied in simulations 2, 3, 4, and 5. The data of the individual runs (that have a different initial path) are shown. Error bars are standard errors from block averaging.

probability to reach the second leaflet is approximately half the crossing probability to reach the first leaflet. Indeed, when ibuprofen is located in the first leaflet, the probability of escaping to the water phase is approximately equal to the probability of overcoming the internal energy barrier towards the second leaflet. This is a direct consequence of the similar magnitudes of the free energy barriers of both (rare) transitions.

sim.	description	interfaces $[\lambda_A, \lambda_1, \ldots, \lambda_B]$ (in nm)	
		run 1 (initial path *cis*)	run 2 (initial path *trans*)
1†*	RETIS entrance	[-3, -2.059, -1.885]	[-3, -2.4, -2.15]
2	RETIS int. barr.	[-1.1, -0.9, -0.75, -0.55, -0.35, 1.2]	[-1.1, -0.9, -0.75, -0.55, -0.35, 1.2]
3	REPPTIS int. barr.	[-1.1, -0.85, -0.69, -0.54, -0.35, 0, 0.35, 0.54, 0.69, 0.85, 1.2]	[-1.1, -0.8, -0.585, -0.449, -0.349, -0.261, -0.171, 0, 0.171, 0.261,0.349, 0.449, 0.585, 0.8, 1.2]
4	RETIS escape	[1.5, 1.75, 1.9, 2.1, 3]	[1.5, 1.75, 1.9, 2.1, 3]
5	REPPTIS escape	[1.5, 1.74, 1.91, 2.1, 3]	[1.5, 1.66, 1.83, 1.98, 2.15, 2.4, 3]
6*	REPPTIS full transit	[-3, -2.059, -1.885, -1.29, -0.885, -0.717, -0.384, 0, 0.384, 0.717]	[-3, -2.4, -2.15, -1.98, -1.83, -1.66, -1.25, -0.8, -0.585, -0.449, -0.349, -0.261, -0.171, 0, 0.171, 0.261]

TABLE S1: Interfaces used in the different RE(PP)TIS simulations. The same λ_A and λ_B interfaces are used in simulations for RETIS as for REPPTIS. This is to ensure that the comparison of the P_{int} values from RETIS and REPPTIS make sense. Wirefencing was used for simulations 2 and 4.

$*$: simulations 1 and 6 use a $\lambda_{-1} = -3.4\,\text{nm}$ interface, while the other simulations use no λ_{-1} interface.

†: Simulation 1 uses a flat free energy region in the water phases, which was implemented by imposing $F(z, \theta) = F(3\,\text{nm}, \theta)$, $\forall |z| > 3\,\text{nm}$. This is done to obtain a better estimate for $\tau_{\text{ref},[0-']}$ and ξ. The crossing probabilities of the other simulations do not depend on F in the water phase.

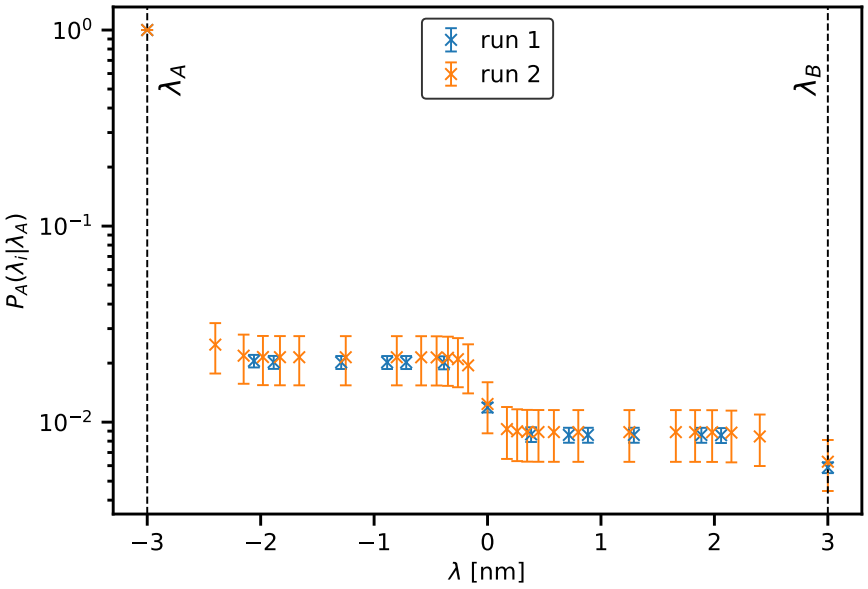

FIG. S8: The REPPTIS crossing probabilities $P_A(\lambda_i|\lambda_A)$ of the full membrane transit of ibuprofen, for the first (blue) and second (orange) runs. Due to *cis-trans* transitions, the dihedral angle configuration of the initial path has no effect on the end results. Error bars are standard errors from block averaging.

D. Markov model for permeation

As RETIS cannot be used for the full transit, the crossing probability of the full transition P_{trans} can be approximated using a Markov model. The Markov model consists of 4 states, which are vizualized in Fig. S9. State A and D are the left and right water phases, respectively. State B and C are the free energy minima in the first and second leaflets, respectively. Let P_{XY} denote the probability of going from state X to a neighbouring state Y. Let $P\left(\begin{smallmatrix} C \\ A \end{smallmatrix} \middle| B\right)$ denote the probability of reaching C for the first time, given that you are in B, and without passing through A. Similarly, let $P\left(\begin{smallmatrix} D \\ A \end{smallmatrix} \middle| C\right)$ denote the probability of reaching D for the first time, given that you are in C, and without passing through A. The full transit probability P_{trans} is then approximated by

$$P_{\text{trans}} = P_{AB} P\left(\begin{smallmatrix} C \\ A \end{smallmatrix} \middle| B\right) P\left(\begin{smallmatrix} D \\ A \end{smallmatrix} \middle| C\right). \tag{3}$$

$P\left(\begin{smallmatrix} C \\ A \end{smallmatrix} \middle| B\right)$ is simply given by P_{BC}, while $P\left(\begin{smallmatrix} D \\ A \end{smallmatrix} \middle| C\right)$ is found using a recursive relation

$$P\left(\begin{smallmatrix} D \\ A \end{smallmatrix} \middle| C\right) = P_{CB} P\left(\begin{smallmatrix} C \\ A \end{smallmatrix} \middle| B\right) P\left(\begin{smallmatrix} D \\ A \end{smallmatrix} \middle| C\right) + P_{CD}.$$

Substituting P_{BC} for $P\left(\begin{smallmatrix} C \\ A \end{smallmatrix} \middle| B\right)$, gives

$$P\left(\begin{smallmatrix} D \\ A \end{smallmatrix} \middle| C\right) = \frac{P_{CD}}{1 - P_{CB} P_{BC}}. \tag{4}$$

Plugging these expressions into Eq. 3, the transit probability is given by

$$P_{\text{transit}} = \frac{P_{AB} P_{BC} P_{CD}}{1 - P_{CB} P_{BC}}. \tag{5}$$

The relation between the transition probabilities P_{XY} and the characteristic crossing probabilities is now described. The entrance probability directly gives $P_{AB} = P_{DC} = P_{\text{entr}}$, where the first equality holds due to symmetry. The transition probabilities P_{BA} and $P_{BC} = 1 - P_{BA}$ are given by the relative ratios of the corresponding rates

$$\begin{cases} P_{BA} = \dfrac{k_{BA}}{k_{BA} + k_{BC}} = \dfrac{k_{\text{esc}}}{k_{\text{esc}} + k_{\text{int}}}, \\ P_{BC} = \dfrac{k_{BC}}{k_{BA} + k_{BC}} = \dfrac{k_{\text{int}}}{k_{\text{esc}} + k_{\text{int}}}. \end{cases}$$

Due to symmetry, $P_{BC} = P_{CB}$ and $P_{CD} = P_{BA}$. Plugging the values of the transition probabilities into Eq. 3, the final expression for the transit probability is obtained

$$P_{\text{trans}} = \frac{P_{\text{entr}} k_{\text{int}}}{k_{\text{esc}} + 2k_{\text{int}}}. \tag{6}$$

The rates k_{esc} and k_{int} are found by multiplying the crossing probabilities P_{esc} and P_{int} with their respective fluxes f_{esc} and f_{int}

$$\begin{cases} k_{\text{int}} = f_{\text{int}} P_{\text{int}}, \\ k_{\text{esc}} = f_{\text{esc}} P_{\text{esc}}. \end{cases}$$

This final step is not required, as the rate – together with the flux and crossing probability – are part of the RETIS output.

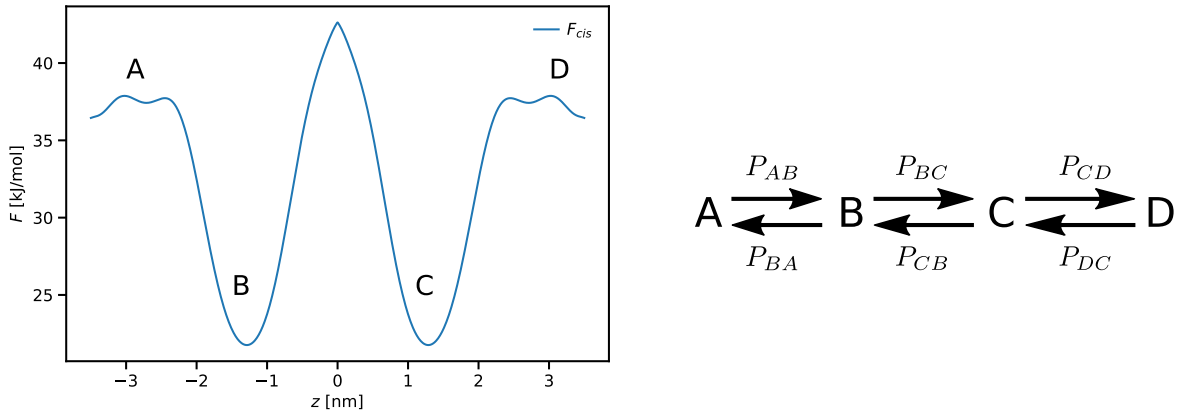

FIG. S9: The 4 states of the Markov model (left) and the transition probabilities between those states (right).

REFERENCES

[1]L. Verlet, "Computer experiments on classical fluids. I. Thermodynamical properties of Lennard-Jones molecules," *Phys. Rev.*, vol. 159, pp. 98–103, 1967.

[2]J. P. Jambeck and A. P. Lyubartsev, "Exploring the free energy landscape of solutes embedded in lipid bilayers," *The Journal of Physical Chemistry Letters*, vol. 4, no. 11, pp. 1781–1787, 2013.

[3]R. Pastor, B. Brooks, and A. Szabo, "An analysis of the accuracy of Langevin and molecular-dynamics algorithms," *Mol. Phys.*, vol. 65, no. 6, pp. 1409–1419, 1988.